UNIVERSITÀ DEGLI STUDI DI PADOVA

DIPARTIMENTO DI FISICA ED ASTRONOMIA "Galileo Galilei"
DIPARTIMENTO DI INGEGNERIA DELL'INFORMAZIONE

CORSO DI LAUREA MAGISTRALE IN FISICA

Quantum Communications with Hyper-entangled states between indipendent terminals

RELATORE: prof. Paolo Villoresi
CORRELATORE: dott. Giuseppe Vallone
CONTRORELATORE: dott. Marco Bazzan

LAUREANDO: Francesco Raffaelli

Anno Accademico 2013/2014

Contents

Sommario

Dalla nascita della Meccanica Quantistica, all'inizio del XX secolo, un gran numero di scienziati si è impegnato allo scopo di comprendere alcuni suoi aspetti di difficile interpretazione. Molti problemi riguardavano il concetto di entanglement, la proprietà di correlazione di alcuni sistemi fisici, la quale non possiede alcun corrispettivo classico. L'idea alla base dell' entanglement è che, dato un insieme di particelle che abbiano interagito in un tempo precedente, una misura operata su parte del sistema andrà ad influenzare in modo *istantaneo* il risultato di una eventuale misura sulla rimanente parte del sistema, indipendentemente dalla distanza presente tra le particelle di tale sistema. Questo fatto implica che i sistemi quantistici possono presentare caratteristiche di *non-località*. Da un punto di vista matematico, gli stati complessivi di sistemi entangled saranno definiti stati *non separabili*, cioè stati quantistici che non possono essere scritti come prodotto tra stati di particella singola.
Accanto ad aspetti di natura fondamentale, nel corso degli anni '80 alcuni scienziati osservarono come la meccanica quantistica potesse essere sfruttata nel campo delle comunicazioni e della computer science. Nacque l'*Informazione Quantistica*.
In particolare, il mio lavoro di tesi rientra nell'ambito delle *Comunicazioni Quantistiche*, le quali sfruttano le proprietà fisiche dei sistemi quantistici per ottenere protocolli di comunicazione che superano i protocolli di comunicazione classici. Di particolare interesse sono i protocolli di *Quantum Key Distribution* (QKD), *Dense Coding* e il *teletrasporto quantistico*. Parlando di comunicazioni, risulta di fondamentale importanza poter trasmettere l'informazione voluta attraverso grandi distanze e questo è possibile grazie alle comunicazioni quantistiche in free-space. Negli ultimi anni diversi esperimenti sono stati realizzati in questo senso e gli esperimenti terrestri con le distanze maggiori sono stati realizzati presso le Isole Canarie tra Tenerife e La Palma, ad una distanza di 144 km [13],[12].
L'obbiettivo del mio lavoro è dunque quello di realizzare comunicazioni quantistiche basate su stati hyper-entangled, cioè stati fotonici entangled simultaneamente in differenti gradi di libertà. Il grande vantaggio dell'hyper-entanglement è che esso permette di codificare una grande quantità di informazione, in forma di bit quantistici, in diversi gradi di libertà. Dunque, dato un numero fissato di fotoni, uno stato hyper-entangled permetterà di inviare una quantità di informazione superiore a quella possibile per un stato entangled in un singolo grado di libertà. Nel mio caso particolare, mi concentrerò sulla generazione di stati entangled in polarizzazione e time-bin. Accanto alla polarizzazione, che è probabilmente il metodo più comune di codificare l'informazione quantistica, il time-bin è utile in quanto gli stati quantistici di time-bin

possono essere preservati attraverso grandi distanze in atmosfera. Ora riporto un breve riassunto riguardante il mio lavoro.

Nel primo capitolo andrò a descrivere alcuni concetti basilari di Informazione Quantistica, con un focus particolare sui protocolli di crittografia quantistica, teletrasporto quantistico, dense coding ed entanglement swapping.
Nel secondo capitolo parlerò dell' *hyper-entanglement* discutendo la sua utilità e alcune possibili applicazioni. Successivamente introdurrò alcuni strumenti teorici e sperimentali utili ad affrontare la generazione di stati entangled. In un primo momento mi concentrerò sulla teoria sottostante la *Spontaneous Parametric Down Conversion* che utilizzo per generare l' entanglement in polarizzazione. Nella seconda parte del capitolo entrerò nei dettagli della generazione sperimentale degli stati hyper-entangled, attraverso un'accurata descrizione del set up sperimentale.
Nel terzo capitolo mi concentrerò sul metodo utilizzato per ricostruire gli stati hyper-entangled. Inizialmente descriverò separatamente le misure in time-bin e polarizzazione da un punto di vista teorico. Dopo affronterò alcune problematiche connesse alle misure degli stati di time-bin, come il modo in cui definiamo le *coincidenze* e quei problemi associati alla stabilità degli intereferometri. In seguito descriverò nei dettagli le tecniche utilizzate per la sincronizzazione, metodo utilizzato per ricavare i conteggi dai terminali di misura separati e indipendenti. La sincronizzazione gioca un ruolo centrale in questo tipo di esperimenti in quanto, in particolare per le misure degli stati di time-bin, è richiesta una grande precisione sulle misure temporali. Concluderò questo capitolo introducendo alcuni concetti riguardanti le matrici densità per gli stati quantistici e i metodi utilizzati per ricostruire tali matrici.
Nell'ultimo capitolo andrò a riportare i risultati sperimentali ottenuti a conclusione di questo progetto. Misurerò la Disuguaglianza di Bell per gli stati di polarizzazione e tempo, separatamente. Successivamente farò alcune tomografie quantistiche, ancora una volta con gli stati di polarizzazione e tempo trattati separatamente, utilizzando il metodo di Maximum Likelihood. Come ultima cosa misurerò una tomografia quantistica per lo stato hyper-entangled. In questo caso utilizzerò i metodi di Compressive Sensing per ricostruire la matrice densità.

Abstract

Since its birth, at the beginning of the XX century, a lot of scientists struggled to understand and interpret some difficult theoretical aspects related with Quantum Mechanics. Most problems were related with *entanglement*, which is a correlation property of some many particles systems that has no classical analogue. The basic idea of entanglement is that if we have some particles that have been interacting before, a measure performed on a part of the system will influence *istantaneously* the results of a measure on the remaining part, no matter what is the distance between the particles of such a system. This fact implies that quantum systems have *non-local* features. From a mathematical point of view we will say that an *entangled* system's state is *non-separable*, which means that this state cannot be written as a product of single particle's states.
Furthermore, during the '80 some scientists understood that quantum mechanics could be exploited in the field of communications and computer science, overcoming classical results. It was the start of *Quantum Information*.
My work, in particular, deal with *Quantum Communications*, which exploit the physical properties of some quantum systems to achieve communications protocols able to overcome classical communications' methods. There are many interesting protocols such as *Quantum Key Distribution* (QKD), *Quantum Teleportation* and *Dense Coding*, provide a great number of advantages in comparison with classical communication systems. Discussing about communications, it is important to exchange information along great distances. This is possible thanks to *free-space* quantum communications. Many experiment have been performed in the latest years in free-space. The experiments with the largest terrestrial distance were performed at the Canaries Islands along 144 km, between Tenerife and La Palma, [13],[12].
The goal of my work is to perform quantum communications based on *hyper-entagled* photons, that are photons entangled, at the same time, in different degrees of freedom. The great advantage of hyper-entangled is that it allows to encode a greater amount of information, in the form of *quantum bits* in different degrees of freedom. Thus, given a fixed number of photons, an hyper-entangled state will allow to send more qubits than a single DOF entangled state.
In this project I create photons entangled both in polarization and time-bin. Beside polarization, which is probably the most common way to encode quantum information, the time-bin is important as time-bin states can be easily preserved along great distances throught the atmosphere and free-space in general. Here a brief summary is reported.
In the first chapter I will describe some basic concepts related with Quantum Information, with

a particular focus on quantum cryptography and other quantum communication protocols such as *quantum teleportation*, *dense coding* and *entanglement swapping*.
In the second chapter I will talk about *hyper-entanglement* discussing its advantages and possible applications in quantum communications. I will then describe the theoretical and experimental tools useful to face with entanglement generation. At first I will deal with the quantum theory underlying *Spontaneous Parametric Down Conversion*, that I exploit to generate polarization entanglement. In the second part I enter some details about the set up used to generated hyper-entangled photons.
In the third chapter I will concentrate on the method used to recover the hyper-entangled photons. At first I will distinguish between polarization and time-bin's measurements, from a theoretical point of view. Then I will face with some issues stricly connected with time-bin measures, such as the way in which we define the *coincidences* and the stability of the interferometers. After this step I will enter some details about synchronization technique, used to recover counts from separated and indipendent terminals. Synchronization plays a central role on this kind of experiments, since, in particular for time-bin measurements, a great precision on time measurement is needed. I will end this chapter introducing some theoretical ideas related with density matrices for quantum states, and the methods used to recover them.
In the last chapter I will report the experimental results obtained in this project. To check the generated states I will measure Bell's Inequality for the different separated states of polarization and time-bin. Then I will perform quantum state tomographies for separated states, by using Maximum Likelihood Estimates. Finally I will perform a complete quantum state tomography for the hyper-entangled state in which polarization and time-bin entanglemed states are considered at the same time. In this case I use the Compressive Sensing technique to recover the density matrix.

Chapter 1

Quantum Information

1.1 EPR paradox and Bell's theorem

1.1.1 EPR Paradox

In 1930 *"The principles of Quantum Mechanics"*, written by Paul Dirac, was published. In this book he formalized the work done in the previous decades, concerning with the novel theory of *Quantum Mechanics*. Since the end of XIX century some experimental and theoretical evidences brought scientists to look for the theory that would have changed the way of thinking about physical world.
The phenomenon of *Black Body Radiation*, discovered in 1877, with the later theoretical development by Plank in 1900 led physicists to think about the possibility that, as had happened for electric charge, light was *quantized*. It was then found by Einstein that a quantized light was consistent with a model that was able to explain *Photo-electric Effect*, which had been observed first in 1887 by Hertz. The presence of *spin* observable was demonstrated in 1922 by Stern and Gerlach that showed that spin got only *quantized values* and that it coupled with magnetic field. In 1926 Shrodinger introduced the $Shrödinger\ Equation$ and in 1927 Heisenberg proposed the *Uncertainty Principle*. Thus *Quantum Mechanics* became soon a succesful theory among that group of physicists. However some questions arose, because of the difficult interpretation of some aspects, such as *superposition properties* and *Uncertainty Principle*.
In 1935 Eisten Podolsky and Rosen proposed a tought experiment to show what they felt a paradox in Quantum Mechanics. They made two definitions:
Reality: *if, without in any way disturbing a system, we can predict with certainty (i.e., with probability equal to unity) the value of a physical quantity, then there exists an element of physical reality corresponding to this physical quantity.*
Complete: *Every element of reality must have a counterpart in the physical theory.*

In their article [1] they wrote that this two conditions made a contraddiction with Quantum Mechanics. They argued that:

"Quantum Mechanics is not complete **or** *two non-commuting observables cannot have simultaneous reality."*

In fact, for a single particle quantum state, Heisenberg's Uncertanity Principle says that, given two observables A and B, the following relation holds

$$\langle (\Delta A)^2 (\Delta B)^2 \rangle \geq \frac{|\langle [A,B] \rangle|^2}{4}. \tag{1.1}$$

In the particular case of momentum P and position Q we obtain that

$$\langle (\Delta P)^2 (\Delta Q)^2 \rangle \geq \frac{\hbar}{2}. \tag{1.2}$$

By (1.2) we observe that, if P and Q have simultanous reality, perfect knowledge on P implies a perfect uncertainty on Q and thus uncompleteness of the theory.
Consequently, by this example, Quantum Mechanics must be considered a complete theory only if the non-commuting operators does not have simoultaneous reality. What Einstein wanted to show is that one can obtain non-commuting operators with simoultaneous reality, reaching the conclusion that Quantum Mechanics is not complete. Let us consider the following system. We have two particles that have been interacting in a early time and that at the moment of measurement are distant in space. The total state function is

$$\Psi(x_1, x_2) = \sum_{n=1}^{\infty} \phi_n(x_1)\chi_n(x_2). \tag{1.3}$$

We measure the osservable P of the first particle and obtain the eigenvalue p_k. We leave $\Psi(x_1, x_2)$ in the state $\phi_k(x_1)\chi_k(x_2)$, determining the state $\chi_k(x_2)$ of the second particle without disturbing it. If we write again our state, this time in term of the observable Q, we have

$$\Psi(x_1, x_2) = \sum_{s=1}^{\infty} \phi_s(x_1)\chi_s(x_2). \tag{1.4}$$

We then measure Q of the first particle, obtaining the eigenvalue q_r, then we have left the system in the state $\phi_r(x_1)\chi_r(x_2)$, and we have predicted with certainty the state $\chi_r(x_2)$ of the second particle. Thus, following Einstein argument, we can assert that Q and P have simoultaneous reality, by the above definition. However we know that P and Q are non-commuting operators, hence we are led to conclude that, in this particular case, we deal with non-commuting operators that refer to observables which have simoultaneous reality. This fact implies *Quantum Mechanics is not Complete*.
On one hand the supposed not completenss of Quantum Mechanics brought different physicians to think about the existence of *Hidden Variables* which could complete the theory (following the EPR definition). On the other hand in the EPR experiment we can observe how a

measurement on the first particle let us do a certain and istantaneous prediction on the second particle's observable, regardless the actual distance between the particles. This non-local effect was what Albert Einstein called *"spooky action at a distance"*. We can say that the two particles are **'entangled'** because of the correlation properties of the measurement on them. Below we will give an accurate definition.
It is interesting to note that the above argument is important for an historical point of view. The following discussions on the subject will not have be based on position and momentum observables, but on a different physical system, which is the spin singlet state

$$|\Psi\rangle = \frac{1}{\sqrt{2}} \left[|\uparrow\rangle_A |\downarrow\rangle_B - |\downarrow\rangle_A |\uparrow\rangle_B \right]. \tag{1.5}$$

Here we can see how a measurement on the particle A can give a perfect prediction about the state of the particle B, regardless the distance of the particles.

1.2 Entanglement

Here we give a mathematical definition of entanglement.

Definition 1 ***(Entangled)*** *Consider a two particles' state $|\psi\rangle$, with $|\phi_A\rangle$ and $|\chi_A\rangle$ single particles' states which lie respectively in $\mathcal{H}_A$ and $\mathcal{H}_B$ Hilbert spaces. The particles are entangled if we cannot separate the state $|\psi\rangle$ on the product Hilbert space $\mathcal{H}_A \otimes \mathcal{H}_B$:*

$$|\psi\rangle \neq |\phi_A\rangle \otimes |\chi_B\rangle. \tag{1.6}$$

1.2.1 Bell's Theorem

In 1964 John Bell [2] demonstrated that Local Hidden Variables (LHV) theories cannot reproduce Quantum Mechanics results. He used the singlet state system to approach the problem. Quantum Mechanics calculation predicts that in the most general measurement of two particle's (1.1.1) state we get

$$A(\vec{\alpha}, \vec{\beta}) \equiv \langle \Psi | (\sigma_A \cdot \vec{\alpha})(\sigma_B \cdot \vec{\beta}) | \Psi \rangle = -\vec{\alpha} \cdot \vec{\beta}. \tag{1.7}$$

Considering a particle moving along the z axis and a measurement plane x-y, we obtain

$$A(\alpha, \beta) = -cos(\alpha - \beta), \tag{1.8}$$

with α and β respectively angles between $\vec{\alpha}$ and $\vec{\beta}$ and the x axis. We define the coincidence rate

$$C(\alpha, \beta) = |A(\alpha, \beta)|^2 = |cos(\alpha - \beta)|^2 \tag{1.9}$$

and the parameter $E(\alpha, \beta)$ as

$$E(\alpha, \beta) = \frac{C(\alpha, \beta) - C(\alpha_\perp, \beta) - C(\alpha, \beta_\perp) + C(\alpha_\perp, \beta_\perp)}{C(\alpha, \beta) + C(\alpha_\perp, \beta) + C(\alpha, \beta_\perp) + C(\alpha_\perp, \beta_\perp)}. \tag{1.10}$$

Finally we can define

$$S(\alpha, \beta, \alpha', \beta') = E(\alpha, \beta) - E(\alpha', \beta) + E(\alpha, \beta') + E(\alpha', \beta'). \tag{1.11}$$

We will now demonstrate that for a LHV theory hold the constraints

$$|S(\alpha, \beta, \alpha', \beta')| \leq 2. \tag{1.12}$$

LHV theories deal with the idea that the non-local features of Quantum Mechanics come from one or more hidden variables that somehow determine the relation between the results of measurement on the particles of the system. It makes no difference if we have a single or a set of variables and we write the probability of a measurement as dependent on the angle and the hidden variable λ. We underline that we just want this variable to be local, so a measurement on particle A, will not depend on β angle and viceversa.
I will follow the argument of Clauser et al. article of 1969 [3] which is more suitable with experiments than the original of Bell. Suppose we can detect the particles with the aid of a couple of detectors. We define two functions $A(\lambda, \alpha)$ and $B(\lambda, \beta)$ for the different path of the particles A and B, which can assume the values ± 1. The probability of detecting A (or B) is given by

$$P(\lambda, \alpha) = \int d\lambda \rho(\lambda) \frac{1 + A(\lambda, \alpha)}{2} \tag{1.13}$$

and the probability of detecting both the particles is given

$$P(\lambda, \alpha, \beta) = \int d\lambda \rho(\lambda) \frac{1 + A(\lambda, \alpha)}{2} \frac{1 + B(\lambda, \beta)}{2} \tag{1.14}$$

were $\rho(\lambda)$ is a distribution function on the λ space. Here the probability has the same meaning of the $C(\alpha, \beta)$ function defined above. Thus writing $E(\alpha, \beta)$ in term of the hidden variables λ we obtain

$$E(\lambda, \alpha, \beta) = \int d\lambda \rho(\lambda) A(\lambda, \alpha) B(\lambda, \beta). \tag{1.15}$$

Under the hypotesis that $\rho(\lambda)$ is a normalized distribution, it is easy to show that the inequality (1.12) holds. In fact, for all the possible combinations of the α and β angles we get a maximum value of the integral equal or minor than one. Since we are summing three and subtracting one of them, it results that the maximum value of $S(\alpha, \beta, \alpha', \beta')$ is two. This is not the case of Quantum Mechanics predictions, which for a suitable choice of the angles can give

$$S(\alpha, \beta, \alpha', \beta') = \pm 2\sqrt{2}. \tag{1.16}$$

Thus, in principle, if one would be able to built up an experiment that allows to measure the coincidences rates varying α and β, he could distinguish between quantum and classical systems. Different experiments were made with this goal. It is important to quote Aspect et al. which in 1982 [4] used polarization as observable for the two particle system. Other experiments of interest are surely that by Franson of 1989 [5] which measured energy-time.

1.3 Quantum Protocols

In the first section we have described the fundamental questions that arose during the first decades of Quantum Mechanics. In this one we will deal with the possible applications that derived from this new physical theory. These applications are strictly related to the progress of information technology. We will see how entanglement became the striking feature to get over the classical information.
In classical information theory we have that a two levels system can carry a 1 bit maximum information. If we have a quantum system things change. We can assert that the new possibilities lie in the superposition properties of Quantum Mechanics. Suppose we have a two levels system, an atom with a ground and an excited level, or a vertical or horizontal polarized photon. Then the state will be written as

$$|\psi\rangle = a|0\rangle + b|1\rangle. \tag{1.17}$$

The state is no more $|0\rangle$ or $|1\rangle$, but it is a superposition of them. In this way we can represent simultaneously two values in a single quantum bit. To show the great possibilities of the superposition properties consider, for example, four quantum bits. The global state will be a linear combination of the different states, which will be a 16 terms state:

$$\begin{aligned} |\psi\rangle &= \frac{1}{4}(|0000\rangle + |0001\rangle + |0010\rangle + |0100\rangle \\ &+ |1000\rangle + |0011\rangle + |0110\rangle + |1100\rangle \\ &+ |0111\rangle + |1110\rangle + |1111\rangle + |1001\rangle \\ &+ |1010\rangle + |0101\rangle + |1011\rangle + |1101\rangle). \end{aligned} \tag{1.18}$$

A unitary transformation on such a system will work at one on 2^4 binary states. Thus, with quantum bits, one can resolve problems exponentially faster than with classical bits.

1.3.1 Dense Coding

As anticipated in the previous sections quantum bits allow one to carry more information with respect to the classical case. In 1995 A. Zeilinger et al. [6] demonstrated this fact experimentally. They showed they were able to send a message using "15 trit" instead of 24 classical bits. By using polarization entangled photons they were able to increase the channel capacity from

1 bit to $\log_2 3 = 1.583$ bit. The basic idea of their experiment was that entangled particles behave differently as long as they are in a different Bell's state. Hence one can manipulate the states and distinguish among them. We remind that, given two photons A and B, Bell's states are defined as follows

$$|\Psi^{\pm}\rangle = \frac{1}{\sqrt{2}}\left(|H\rangle_A|V\rangle_B \pm |V\rangle_A|H\rangle_B\right)$$
$$|\Phi^{\pm}\rangle = \frac{1}{\sqrt{2}}\left(|H\rangle_A|H\rangle_B \pm |V\rangle_A|V\rangle_B\right). \tag{1.19}$$

They generated the state $|\Psi^+\rangle$ and then sent the first photon to Bob, and the second one to Alice. Bob works on the photon B making a unitary transformation which transforms $|\Psi^+\rangle$ in one of the Bell's states, while Alice detects the photons and distinguish the different states. The transformation that Bob operates are:

- Unitary transformation which leaves the state unchanged;
- Phase-indipendent rotation of polarization which gives $|\Phi^+\rangle$;
- Phase retarding which gives $|\Psi^-\rangle$;
- Phase-dependent rotation which gives $|\Phi^-\rangle$.

Thus he obtains three symmetric states under the change of the photons, and one state, $|\Psi^-\rangle$, which is antisymmetric. This first observation allows Alice to distinguish $|\Psi^-\rangle$ state from the others. It suffices to put a polarization indipendent beam splitter on the path of the photons. Ou-Mandel effect tells us that for an antisymmetric state photons will emerge on different sides of the beam splitter, while for a symmetric state, such as $|\Phi^{\pm}\rangle$ and $|\Psi^+\rangle$, photons will emerge on the same side. Therefore $|\Psi^-\rangle$ will be determined by detecting, with reference to fig. (1.1), one photon in the upper detectors and the other in the lower ones. In the second step Alice must separate the symmetric states. She uses a polarizing beam splitter which trasmits one polarization and reflects the orthogonal one. In this way she will have $|\Psi^+\rangle$ characterized by photons directed on different detectors and $|\Phi^{\pm}\rangle$ with photons which will fall on the same detector and will be indistinguishable. Finally the entire system allows Alice and Bob to have three different signals given by the detection of $|\Phi^{\pm}\rangle$, $|\Psi^-\rangle$ and $|\Psi^+\rangle$. This experiment showed a great possibility of enanching channel capacity with respect to classical systems. Furthermore we note that *Entanglement* plays an important role on this application.

1.3.2 Quantum Teleportation

The most amazing possibility of Quantum Mechanics is, with no doubt, *Quantum teleportation*, ideated in 1993 [7] and realized in 1997 [8]. The basic idea of this protocol is that, under the hypotesis that Alice and Bob share an entangled state, then Alice will be able to teleport a given single photon state

$$|\psi\rangle = c_0|0\rangle + c_1|1\rangle, \tag{1.20}$$

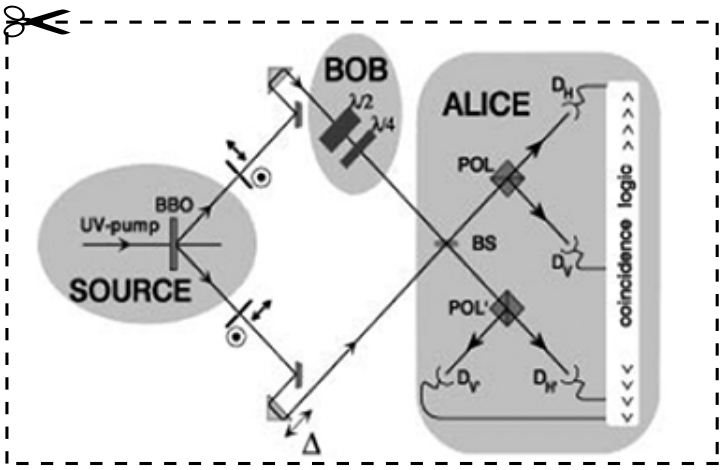

Figure 1.1: Dense Coding first experiment, original setup extracted from 1995 article.

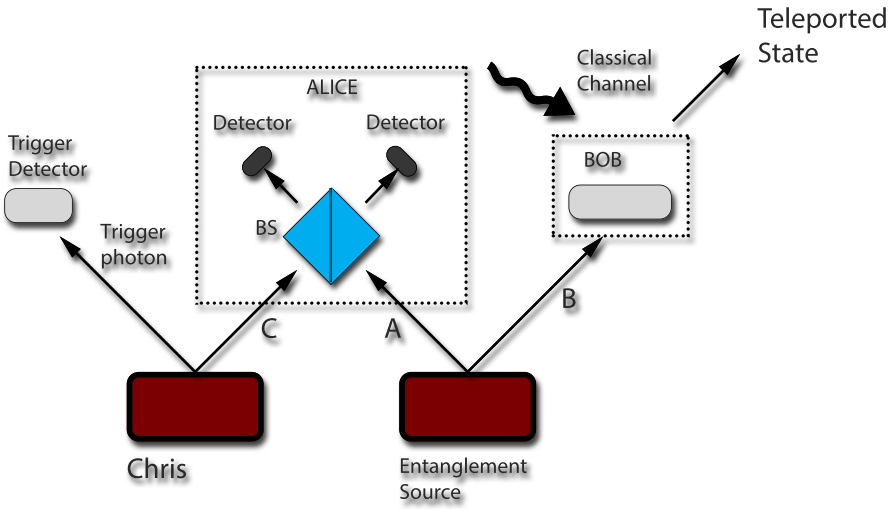

Figure 1.2: Here the scheme of teleportation protocol.

to Bob. Suppose that, beside $|\psi\rangle$, Alice possesses part of a state entangled with Bob, that is maybe provided by a thirt part Chris. The entangled state is

$$|\Psi^-\rangle_{AB} = \frac{1}{\sqrt{2}} \left(|0\rangle_A |1\rangle_B - |1\rangle_A |0\rangle_B \right), \tag{1.21}$$

where $\{|0\rangle, |1\rangle\}$ is a generic set of eigenstates of a two-states system, that could have any physical experimental realization, such as polarization photon state or atomic levels. Then we can write the total system state as

$$|\chi\rangle \equiv |\psi\rangle \otimes |\Psi^-\rangle_{AB}. \tag{1.22}$$

Before going on, it is useful to write $|\chi\rangle$ in a more suitable form as

$$\begin{aligned} |\chi\rangle &= \frac{1}{\sqrt{2}} \left[c_0|0\rangle|0\rangle_A|1\rangle_B - c_0|0\rangle|1\rangle_A|0\rangle_B + c_1|1\rangle|0\rangle_A|1\rangle_B - c_0|1\rangle|1\rangle_A|0\rangle_B \right] \\ &= \frac{1}{2} \left[|\psi^-\rangle \left(c_0|0\rangle_B + c_1|1\rangle_B \right) + |\psi^+\rangle \left(c_0|0\rangle_B - c_1|1\rangle_B \right) \right] \\ &+ \frac{1}{2} \left[|\phi^-\rangle \left(c_0|1\rangle_B + c_1|0\rangle_B \right) + |\phi^+\rangle \left(c_0|1\rangle_B - c_1|0\rangle_B \right) \right], \end{aligned} \tag{1.23}$$

where we have introduced the four Bell states in which we have entangled Alice's particles. We remember that Alice has a particle related to $|\psi\rangle$ state and another one belonging to the original entangled state. Writing the global state in this way implies that, as we have said, Alice's particles are entangled and can be expressed as

$$\begin{aligned} |\psi^\pm\rangle &= \frac{1}{\sqrt{2}} \left(|H\rangle|V\rangle_A \pm |V\rangle|H\rangle_A \right) \\ |\phi^\pm\rangle &= \frac{1}{\sqrt{2}} \left(|H\rangle|H\rangle_A \pm |V\rangle|V\rangle_A \right). \end{aligned} \tag{1.24}$$

This result is obtained by making Alice's particles indistinguishable with the aid of a PBS and two detectors, one for each output. Coincidence detections mean that the Bell state $|\psi^-\rangle$ has been generated. Looking again at (1.24) now we observe that any state measurement by Alice will project Bob's photon on a defined state. If Alice finds $|\psi^-\rangle$ then Bob will find Alice's original state and we can say that Alice has teleported her state to Bob. If Alice measures one of the other Bell's states, then Bob can always recover Alice's original state by working locally on his photon. In this second situation we have to admit classical communication between Alice and Bob in which Alice tells Bob her measurement's result. We note that, thanks to entanglement, local manipulations modify the whole system, no matter how distant are Alice and Bob. This is a common feature of quantum protocols.

1.3.3 Entanglement Swapping

Another interesting protocol is **Entanglement Swapping** in which, with a set up similar to that of teleportation, it is possible to entangle particles that had never interacted before. Looking

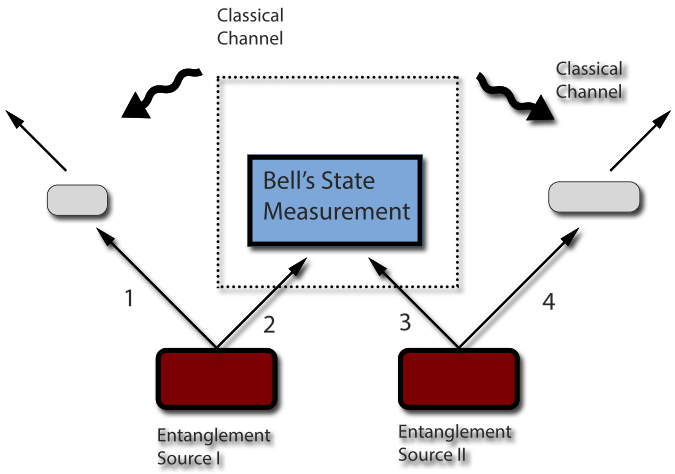

Figure 1.3: Here the scheme of entanglement swapping. We can note a set up similar to that of teleportation. Howevere, the trigger photon of teleportation now is entangled with one photon of the main source. This is achieved by performing a Bell's state measurement between one photon from each pair of entangled photons.

at fig. (1.3) we observe that Chris also generated an entangled pair, using one of the photons as a trigger to check the presence of the photon that interact with that of Alice. Entaglement swapping exploits the trigger photon in a different way. Now we enter some details of such protocol. Consider two sources of entangled photons, and the entangled states

$$|\psi^-\rangle_{12} = \frac{1}{\sqrt{2}}\left(|H\rangle_1|V\rangle_2 - |V\rangle_1|H\rangle_2\right) \tag{1.25}$$

$$|\psi^-\rangle_{34} = \frac{1}{\sqrt{2}}\left(|H\rangle_3|V\rangle_4 - |V\rangle_3|H\rangle_4\right). \tag{1.26}$$

The four particles global state is then

$$|\chi\rangle_{1234} = \frac{1}{2}\left(|H\rangle_1|V\rangle_2 - |V\rangle_1|H\rangle_2\right) \otimes \left(|H\rangle_3|V\rangle_4 - |V\rangle_3|H\rangle_4\right), \tag{1.27}$$

and can be written as

$$|\chi\rangle_{1234} = \frac{1}{2}\left(|\psi^-\rangle_{14}|\psi^-\rangle_{23} + |\psi^+\rangle_{14}|\psi^+\rangle_{23} + |\phi^-\rangle_{14}|\phi^-\rangle_{23} + |\phi^+\rangle_{14}|\phi^+\rangle_{23}\right). \tag{1.28}$$

Thus, projecting particle 2 and 3 on one of the Bells' states, we will entangle particle 1 and 4, nevertheless they had never interacted before. As noted before, this scheme is achieved with as similar apparatus to that of teleportation. Such experiment as been realized first in 1998 by Pan et al. [9].

1.3.4 Quantum Cryptography

Classical Cryptography: RSA

Secure communication has always been a subject of great interest along human kind history. In the XX century, with the development of information and modern communication technologies, his role has achieved more importance. Different methods of sharing secure information have been invented, and perhaps the most popular classical cryptographic system has become **RSA**. Here we will briefly describe how such a protocol works, just to give an idea of the matter we deal with. The problem we face with is that of Alice and Bob who want to exchange a private message *m*. We can summarize the process as follows:

- Bob creates the *public key* by choosing two prime numbers q and p, greater than 10^{1000} and calculates $N = p * q$ and $f(N) = (p-1) * (q-1)$;
- he then chooses a *coprime* number e with $f(N)$ and defines $d = e^{-1}\ mod(f(N))$.
- he sends to Alice the *public key* (e,N);
- Alice receives the *public key* and she uses it to encode her secret message m computing $c = m^e\ mod(N)$;
- Alice sends her encrypted message to Bob who reads it by using his *private key* (d,N). Bob calculates $m = c^d\ mod(n)$ and obtain Alice's message.

We have described some details of a classical cryptographic method to look at his features. We immediately see that the only difficulty on decrypting such a message by an eavesdropper is related to the size of the prime numbers of the key. It has been demonstrated that classical computers need a long time (probably months) to find q and p that are necessary for reading the message. This is the reason of the RSA protocol's success. However it has been shown that a computer based on quantum algorithms would work exponentially faster than a classical one. Such a technology would then threaten the security of RSA and other protocols which are based on computation limits of actual computers. It is thus important to find intrinsecally secure cryptographic protocols. Here lies the importance of Quantum Cryptography. In the next paragraphs we will describe some Quantum Cryptography protocols.

"No-cloning theorem" Before showing some protocols we describe the so called *No-cloning theorem* which is perhaps the most important quantum mechanics' tool we deal with, talking about Quantum Cryptography. Roughly speaking, *No-cloning theorem* tells us that a quantum state cannot be copied preserving its properties. We use a simple example to show this point: consider the general state

$$|\psi\rangle = a|0\rangle + b|1\rangle. \tag{1.29}$$

Suppose our goal is to get a copy of this state, whose coefficent a and b are unknown. We operate a unitary transformation U which makes a clone of the $|0\rangle$, $|1\rangle$ states,

$$\begin{aligned} U|0\rangle &\equiv |0\rangle|0\rangle \\ U|1\rangle &\equiv |1\rangle|1\rangle. \end{aligned} \tag{1.30}$$

The linearity of U implies that

$$\begin{aligned} U|\psi\rangle &= U(a|0\rangle + b|1\rangle) \\ &= a|0\rangle|0\rangle + b|1\rangle|1\rangle. \end{aligned} \tag{1.31}$$

On the other hand we have

$$\begin{aligned} U|\psi\rangle &= |\psi\rangle|\psi\rangle \\ &= a^2|0\rangle|0\rangle + b^2|1\rangle|1\rangle + ab|0\rangle|1\rangle + ba|1\rangle|0\rangle. \end{aligned} \tag{1.32}$$

Note that no choice of a and b allows (1.32) to equal (1.31). This is the reason why Eve, the eavesdropper, is unable to get Alice's photons without being discovered.

BB84 Protocol

The first protocol we describe is BB84 [10]. In this protocol Alice sends photons to Bob to test the presence of a possible eavesdropper between their communication channel. Alice generates photons in one of the states

$$\begin{aligned} |\Psi_0\rangle &= |0\rangle \\ |\Psi_1\rangle &= |1\rangle \\ |\Psi_+\rangle &= \frac{1}{\sqrt{2}}\left(|0\rangle + |1\rangle\right) \\ |\Psi_-\rangle &= \frac{1}{\sqrt{2}}\left(|0\rangle - |1\rangle\right). \end{aligned} \tag{1.33}$$

She encode information in the rectilinear base $\{|\Psi_0\rangle, |\Psi_1\rangle\}$ or in the diagonal base $\{|\Psi_+\rangle, |\Psi_-\rangle\}$. In the rectilinear base, $|\Psi_{0(1)}\rangle$ corresponds to the 0 (1) value while, for example, in the diagonal base, $|\Psi_{+(-)}\rangle$ corresponds to the 0 (1) value. She sends her sequence of photons by varying bases and values. Bob receives the photons and tries to get some information on them. He measures the photons' states in one of the bases, chosen at random. They use a public channel, such as a telephone, to share what base they have used for each photon and keep just the photons for which Alice and Bob's bases were the same, discarting all the other photons. Moreover Alice discarts all the photons that, for any reason, did not reach Bob. In the next step they take some photons measured on the same base and check the state to be the same. Finally, they use the remaining photons as the key. To show BB84 protocol we use the table (1.1).

A state	$\|\Psi_0\rangle$	$\|\Psi_-\rangle$	$\|\Psi_1\rangle$	$\|\Psi_-\rangle$	$\|\Psi_0\rangle$	$\|\Psi_1\rangle$	$\|\Psi_-\rangle$	$\|\Psi_+\rangle$	$\|\Psi_1\rangle$	$\|\Psi_+\rangle$	$\|\Psi_1\rangle$
A base	R	D	R	D	R	R	D	D	R	D	R
A value	0	0	1	0	0	1	0	1	1	1	1
B base	D	D	R	R	R	D	R	D	R	D	D
B state	$\|\Psi_+\rangle$	$\|\Psi_-\rangle$	$\|\Psi_1\rangle$	$\|\Psi_0\rangle$	$\|\Psi_0\rangle$	$\|\Psi_+\rangle$	$\|\Psi_1\rangle$	$\|\Psi_+\rangle$	$\|\Psi_1\rangle$	$\|\Psi_+\rangle$	$\|\Psi_+\rangle$
B value	0	0	1	0	0	1	1	1	1	1	1
Ok base		x	x		x			x	x	x	
Test Phot.		0						1			
Key Phot.			1		0				1	1	

Table 1.1: Scheme of BB84 protocol.

We have not talked about the eavesdropper (Eve) yet. Someone could ask what would happen if Eve tries to get some information on the key. Suppose she gets Alice's photons. She must measure their state using one of the two bases, the rectilinear or the diagonal one. If she guesses the right base, namely the same of Alice, she would get the correct value 0 or 1. But she has a 50% probability of taking the wrong choice. Furthermore she has to send to Bob a copy of the photons she measured. These copies however are not the same photons she received from Alice, and if Eve chooses the wrong base Bob would have a 50% probability of getting the wrong value, with the same base of Alice. In this case Bob would suspect about the presence of Eve and would stop the communication with Alice. Thus Eve has a 25% probability of stealing a single photon with success. For Alice and Bob would be enuogh to share a great number of photon to look for the presence of Eve. If she has tried to look at the key, Bob will find about a 25% of wrong values using test photons.

B92 Protocol We are going to present here another QKD protocol which uses two non-orthogonal bases, $R = \{|H\rangle, |V\rangle\}$ or $D = \{|+\rangle, |-\rangle\}$ [11]. Alice and Bob want to share a secret key, checking for the presence of Eve, who is trying to steal the secret key. The protocol works as follows: Alice randomly chooses a base by generating a random sequence of bits 0 or 1. If she gets 0 then she sends the $|H\rangle$ state, vice versa she sends $|+\rangle$. Bob works in the same way: he generates a random sequence of bits and his measurement base will depend on the bit's value. If he obtains 0 then he will use the projection operator $P_H = 1 - |+\rangle\langle+|$ while

when he gets 1 he will use $P_+ = 1 - |H\rangle\langle H|$. Easy calculations allow one to demonstrate that, for example, P_H annihilate the $|+\rangle$ state:

$$\begin{aligned} P_H|+\rangle &= (1 - |+\rangle\langle +|)\,|+\rangle \\ &= |+\rangle - |+\rangle\langle +|+\rangle \\ &= |+\rangle - |+\rangle = 0. \end{aligned}$$

After measuring polarization states, Bob and Alice keep just the photons which gave the value 1 and discart all other photons. As before, due to low efficiency or external factors, some photon will not be detected by Bob, and Alice discarts her corrisponding photons too. It easy to show, as in table (1.2), that, in absence of Eve, the remaining photons will represent the same key for Alice and Bob. As in BB84 protocol Alice and Bob need to sacrify some photons to check Eve is not there. It is interesting, dealing with a cryptographic protocol, to look at

A rnd bits	1	0	0	0	1	1	0	1	1	0	0
A state	$\|\Psi_+\rangle$	$\|\Psi_H\rangle$	$\|\Psi_H\rangle$	$\|\Psi_H\rangle$	$\|\Psi_+\rangle$	$\|\Psi_+\rangle$	$\|\Psi_H\rangle$	$\|\Psi_+\rangle$	$\|\Psi_+\rangle$	$\|\Psi_H\rangle$	$\|\Psi_H\rangle$
B rnd bits	1	0	1	0	0	1	1	1	0	0	0
B meas.	P_1	P_0	P_1	P_0	P_0	P_1	P_1	P_1	P_0	P_0	P_0
B results	1	1	0	1	0	1	0	1	0	1	1
B "1"	1	1		1		1		1		1	1
Test Phot.		1								0	
Key Phot.	1			0		1		1			1

Table 1.2: Scheme of B92 protocol.

the action of Eve. She would try to measure the photons that Alice is sending to Bob. If she randomly chooses the right base she will send to Bob the correct polarization photons and he will not suspect about her presence.
Nevertheless she has a 50% to choose the wrong base. In this case she will send to Bob a different photon. It could happen that, for a 1-value result of Bob, the corresponding bit would be different from the Alice's one. Then Alice and Bob will conclude that Eve is there. Again the intrisic properties of quantum mechanics, related with superposition properties, together with "No-cloning Thereom", make quantum protocols secure agaist possible attacks.

EPR protocol In 1991 Ekert proposed a EPR-paradox based protocol [22]. In this protocol a third party prepares the state

$$|\Psi^-\rangle = \frac{1}{\sqrt{2}}\left(|H\rangle_A|V\rangle_B - |V\rangle_A|H\rangle_B\right) \tag{1.34}$$

sending the first photon to Alice and the second one to Bob. Hence Alice and Bob share an entangled state. They have two sets of measurement angles $\Phi^A = (0, \frac{\pi}{4}, \frac{\pi}{2})$ and $\Phi^B = (\frac{\pi}{4}, \frac{\pi}{2}, \frac{3\pi}{4})$, and randomly choose the measurement angle for each photon they get. They divide their measurement results in two groups: the first one with $\phi_i^A \neq \phi_j^B$ and the second one with $\phi_i^A = \phi_j^B$ (note that $\phi_2^A = \phi_1^B$ and $\phi_3^A = \phi_2^B$). With the first group they make a Bell's measurement to check for the presence of Eve. She could make a polarization measurement on the single photons and replace the photons with others. From chapter 1 we know that Quantum Mechanics predict

$$S = -2\sqrt{2}, \tag{1.35}$$

for this choice of the angles, while from classical theories, such as LHV theories one gets

$$|S| \leq 2. \tag{1.36}$$

Since any action of Eve will introduce an element of physical reality, then, if they get $S = -2\sqrt{2}$, they will ensure that Eve is not there. On the other hand, if they obtain $|S| \leq 2$, they will suspect about the presence of Eve. Thus, with the first group of measurement they are able to test the security of their communications. The violation of Bell's inequalities guarantees also that, with reference to paragraph 1.3, $A(\phi_2^A, \phi_1^B) = A(\phi_3^A, \phi_2^B) = -1$. Thus their random sequences of measurement angles will represent the secret key.
Finally, we have shown some protocols based on entanglement and quantum properties of photons states. We can assert that entanglement plays an central role as it allows to distinguish *quantum* from *classical* and to get over classical limits.

Chapter 2

Hyper-Entanglement: definition and experimental generation

2.1 Introduction to Hyper-entanglement

In the previuos chapters we have shown the great possibilities of quantum entanglement, with a focus on Quantum Communication protocols. We have reported that quantum entangled states allow to increase the quantum channel capacity (Dense Coding experiment) and we have described different QKD protocols which make secret key sharing intrinsecally secure. We have also shown how entanglement can be exploited to teleport quantum states, fact that is useful for many quantum information protocols. In this chapter we will deal with **Hyper-Entanglement**, which concerns with particles that are simultaneously entangled in many degrees of freedom. We will show how this property further enhances quantum technology benefits. Moreover it has been demonstrated that **Hyper-Entanglement** allows us to get over Bell's theorem showing, for example, that LHV theories violation grows up increasing systems size.

Definition 2 *(**Hyper-Entangled**) Two particles are Hyper-Entangled if they are entangled in more than one degree of freedom, namely if, given $\overline{|\phi_A\rangle_j \text{ and } |\phi_B\rangle_j}$, we cannot separate the j-th DOF state $|\psi\rangle_j$:*

$$|\psi\rangle_j \neq |\phi_A\rangle_j \otimes |\chi_B\rangle_j. \quad \forall j. \tag{2.1}$$

Advantages of Hyper-entanglement

The general importance of hyper-entanglement is related to the possibility of encoding a greater information as long as we entangle photons in many degrees of freedom. This is due to the fact that it is possible to perform different measurements for each DOF extracting different information for each degree of freedom. This entails that working with four polarization entangled photons will give us the same information that we can get by working with two photons entangled in two different DOFs (polarization and time, for example). Here we adress to two main pratical advantages one obtains by using particles entangled in many DOFs. We

first focus our attention on **detection** of multi-qubit systems. If we have n two-level particle states, what we need to reveal all particles is n (or more) detectors, one for each particle. Thus, to reveal four polarization-entangled photons, we need at least four detectors. Things change if we employ hyper-entangled states. If we entangle two particles in, for example, time and polarization, we get a four qubit system, with the same size of the four particles states. However in this case we just need two detectors, one for each particle, to obtain the same kind of information. In this way we have reduced the number of detectors, and it can be shown that, in general, working with two level's DOF hyper-entangled states we reduce the number of single photon detectors from n to $\log_2 n$, where n is the number of particles involved. An immediate consequence is that we improve our system efficiency. In fact the detection efficiency of a system is given by η^m, where m is the number of detectors used [14].
Another advantage of hyper-entanglement is related to the problem of **decoherence**. It is obviusly more difficult to avoid decoherence as the number of photons increases. Alignment process is always a challenging part of quantum information experiments, and concentrating more information in a small number of particles makes experiments easier to be done.
To sum up, we can say that hyper-entanglement allows to simplify experiments without changing the basic ideas related with entanglement phenomena. In the next sections we will describe some further possibilities connected with hyper-entangled photons. First we look at quantum mechanics fundaments' experiments and then we will show some applications in quantum information.

Non locality tests

GHZ theorem In this section we deal with non-locality tests based on multi-qubit systems. We first describe GHZ theorem which, for the first time, looked at multi-qubit systems treating non-locality tests. We underline the fact that GHZ theorem deal with entanglement of four particles and not with hyper-entanglement of two particles. However for an historical point of view this theorem is important as it puts new attention on *EPR paradox*.
Bells' theorem asserts that LHV theories cannot reproduce Quantum Mechanics' results, that agree with experimental evidence. Even though Bell's theorem give us a powerful mathematical tool for testing Quantum Mechanic against classical theories, it is easy to show that it has nothing to say about the *'superclassical case'*, namely, when Alice and Bob's measurements' angles differ of $0, \pi$. We note also that EPR-paradox itself was based on a *'superclassical case'* and thus Bell's theorem does not completely answer Einstein's doubts. In 1989 Greenberger, Horne and Anton Zeilinger pointed out that increasing the system's Hilbert space, they would have resolved *'superclassical case'* too. They proceeded as Bell did, just considering a four particles system instead of the two particles spin singlet state. GHZ's state was

$$|\Psi\rangle = \frac{1}{\sqrt{2}} \left(|\uparrow\uparrow\uparrow\uparrow\rangle - |\downarrow\downarrow\downarrow\downarrow\rangle \right), \tag{2.2}$$

and calculations demonstrate that, for particles moving along z-axis and x-y measurement plane,

$$\begin{aligned} A(\vec{\alpha},\vec{\beta},\vec{\gamma},\vec{\delta}) &\equiv \langle\Psi|(\sigma_A\cdot\vec{\alpha})(\sigma_B\cdot\vec{\beta})(\sigma_C\cdot\vec{\gamma})(\sigma_D\cdot\vec{\delta})|\Psi\rangle \\ &= -\cos\left(\alpha+\beta-\gamma-\delta\right). \end{aligned} \tag{2.3}$$

As in EPR thought experiment, measurements on a part of the quantum system give total information about the remaining part. This happens with the condition

$$\begin{aligned} \cos\left(\alpha+\beta-\gamma-\delta\right) &= \pm 1 \\ \Longrightarrow \alpha+\beta-\gamma-\delta &= 0,\pi. \end{aligned} \tag{2.4}$$

In fact it is enough to measure three angles and the fourth will be determined with certainty. After this we can finally move to demonstrate that classical models cannot reproduce, for our four particle system, Quantum Mechanics, neither in the *'superclassical case'*. We introduce the quantity

$$A(\lambda,\alpha)B(\lambda,\beta)C(\lambda,\gamma)A(\lambda,\delta)=\pm 1. \tag{2.5}$$

Under the condition (2.4), fixing two angles, the others will be free of varying with continuity. This entails that A=B=C=D=const, otherwise (2.5) would get continuos values between +1 and -1, that is not physically possible. Then we have been led to a contraddiction, since one cannot have varying results as a product of constant terms. In this way GHZ have demonstrated that LHV cannot reproduce quantum results, neither in the *superclassical* situation [17].

Growing with size non-locality. After these new results, in 1990 Mermin [18] showed that in general, Bell's inequality grows up with the system size. This has been done using a n-particle state similar to that of GHZ:

$$|\Psi\rangle=\frac{1}{\sqrt{2}}\left(|\uparrow_1,..,\uparrow_n\rangle-i|\downarrow_1,..,\downarrow_n\rangle\right), \tag{2.6}$$

and it has been demonstrated that the inequality grows up as $2^{n/2}$. This result is important because it is in contrast with a common idea that Bell's inequality would decrease with a growing size system. In fact they thought that as a system increases its size it should get classical features, that we are used to observe when dealing with a great number of particles. Mermin result tells us that this idea was wrong and, if properly prepared, quantum multi-particles systems will show features very different from classical ones. Even though it has be seen that it is very difficult to generate a state such as (2.6). This fact makes Mermin's result very challenging to demonstrate experimentally.

EPR test with Hyper-entagled states Hyper-entanglement becomes important at this point. It has been shown that, under some assumptions, we can substitute n two-levels system, such as GHZ state, with two n-levels systems. In this way we can simplify experimental set up related to multi-qubit systems. Then, hyper-entanglement became an important tool to test Mermin's observations. Theoretical developments about hyper-entanglement and its connection with Bell's inequality have been studied by Cabello in 2006 [14] and successful experimental tests have been made by Barbieri et al. in 2007.

Hyper-Entanglement for Dense Coding

As we will see *Hyper-entanglement* has been also exploited in Quantum Information.
In section 1.3.1 we have described *Dense Coding* protocol, in which, under some hypothesis, Bob is able to send to Alice more than one bit by working on a single qubit. However, after this result, no further step has been made on this way. This is due to the fact that Bell State Analysis (BSA) with linear optical instruments is unable to distinguish completely the four Bell's states. Moreover current technology does not allow to use non-linear methods to characterize quantum states of photons.
Nevertheless, with the help of hyper-entangled particles Kwiat et al. in 2008 [16], have shown that it is possible to increase quantum channel capacity, overcoming the maximum capacity for a single DOF entangled system. They reached a channel capacity of 1.63, beating the result exposed in section 1.3.1. Even though they did not increase so much channel capacity they showed that hyper-entanglement was a great opportunity to develop Quantum Information technology, related in that case to Dense Coding protocols.

2.2 Non-Linear Optics

Before going to show the hyper-entanglement generation process we will describe two main processes involved in our experiment. These are non-linear processes, that in the latest decades have achieved more and more importance in quantum optics.

BBO crystal and SPDC

As we will see in the next section *Spontaneous Parametric Down Conversion* is probably the most important experimental tool in entangled states generation [19]. For this reason it deserves an accurate description. SPDC is obtained with BBO crystals. We now focus on the **Type-II** crystal. The basic idea is that the incoming photon is splitted into two photons, labeled by e and o, which are entangled in different DOFs. Phase-matching conditions and energy conservation imply that emitted photons will lie on two crossing circles, shifted by an

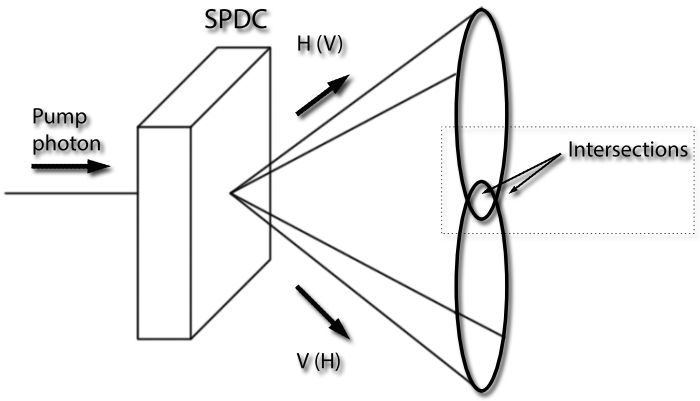

Figure 2.1: BBO and circles generated by SPDC process. The polarization entangled photons are that in the intersection between the two circles. In the intersection one does not know which photon will be H or V.

amount determined by the system properties. We can summarize the process as

$$e \rightarrow e + o. \tag{2.7}$$

We are going to show the quantum theory underlying SPDC processes. We first consider the quantum interaction Hamiltonian between the incoming photon P and the outcoming photons e and o. It can be written as

$$H_I = \int_V \hat{E}_P^{(-)}(\omega_P, \vec{k}_P)\hat{E}_e^{(+)}(\omega_e, \vec{k}_e)\hat{E}_o^{(+)}(\omega_o, \vec{k}_o)d^3\vec{r}, \tag{2.8}$$

where the outcoming photons' electric fields are

$$\hat{E}_j^{(+)}(\omega_j, \vec{k}_j) = \sum_{j=1}^{\infty} E_{j,k_j}\hat{a}_{j,k_j}^{\dagger}e^{i(\omega_{j,k_j}t - \vec{k}_j\cdot\vec{r})}. \tag{2.9}$$

The quantum state is given by first order pertubation theory and is

$$|\Psi\rangle = |0\rangle - \frac{i}{\hbar}\int_{-\infty}^{\infty} H_I dt|0\rangle. \tag{2.10}$$

We now introduce the hypotesis of classical, monochromatic and directed along z pump's electric field, which gives

$$E_P^{(-)}(\omega_P, \vec{k}_P) = E_0 e^{i(k_P z - \omega t)}. \tag{2.11}$$

Furthermore we take $L \to \infty$, and $A \to \infty$, where A is the transverse area of the crystal and L the length along z direction. $|\Psi\rangle$ becomes

$$\begin{aligned} |\Psi\rangle &= |0\rangle - \frac{i}{\hbar}\sum_{k,k'=1}^{\infty}\int_{-\infty}^{\infty} dt \int_V \hat{a}_e^\dagger \hat{a}_o^\dagger e^{i(\omega_e t - \vec{k}_e\cdot\vec{r})} e^{i(\omega_o t - \vec{k}_o\cdot\vec{r})} e^{i(k_P z - \omega t)} \\ &= |0\rangle - \frac{i}{\hbar}\delta_{\omega_P,\omega_e+\omega_o}\delta_{k_P,k_{z,e}+k_{z,o}} \int_A e^{i(\vec{q}_e+\vec{q}_o)\cdot\vec{r}} d^2\vec{r} \\ &= |0\rangle - \frac{i}{\hbar}\delta_{\omega_P,\omega_e+\omega_o}\delta_{k_P,k_{z,e}+k_{z,o}}\delta_{\vec{q}_e,\vec{q}_o}. \end{aligned} \tag{2.12}$$

This implies that three equalities must hold since we want to have a non-zero state:

$$\omega_P = \omega_e + \omega_o \tag{2.13}$$

$$k_P = k_{z,e} + k_{z,o} \tag{2.14}$$

$$\vec{q}_e = -\vec{q}_o. \tag{2.15}$$

It can be useful to start from the collinear situation in which both e and o are directed along the z axis. In this case we take advantage of equation (2.13) and (2.14). Because of birefringence phenonema it can be shown that

$$\begin{aligned} K_e &= \frac{n_e(\Omega_e, \Psi_{OA})\Omega_e}{c} \\ K_o &= \frac{n_o(\Omega_o)\Omega_o}{c} \end{aligned} \tag{2.16}$$

where Ω_e and Ω_o are related to ω_e and ω_o by

$$\begin{aligned} \omega_e &= \Omega_e + \nu_e \\ \omega_o &= \Omega_o + \nu_o, \end{aligned} \tag{2.17}$$

with $\nu_j \ll \Omega_j$. Note that the capital letters always refer to collinear situation. It can be demonstrated also that for ordinary and extraordinary refractive indexes, holds

$$\frac{1}{n_e(\Omega_e, \Psi_{OA})^2} = \frac{\cos^2(\Psi_{OA})}{n_o(\Omega_o)^2} + \frac{\sin^2(\Psi_{OA})}{n_e(\Omega_e)^2}, \tag{2.18}$$

where $n_o(\Omega_o)$ and $n_e(\Omega_e)$ are the longitudinal and transverse refractive indexes, while $n_e(\Omega_e, \Psi_{OA})$ is the extraordinary index, dependent on the angle of the optic axis Ψ_{OA}. After this brief introduction we concentrate on the non-collinear case. We proceed as follows: we define a mis-match function

$$\Delta = k_o + k_e - k_P \tag{2.19}$$

and we find the condition for which this is zero. Because of the different refractive indexes between air and crystal we write the longitudinal component of wave vector as

$$k_{jz} = \sqrt{\left(\frac{n_j\omega_j}{c}\right)^2 - |\vec{q}_j|^2}. \tag{2.20}$$

We expect a small transverse vector $\vec{q}_j$, so, for example, we expand k_{oz} as

$$k_{oz} = \frac{n_o \omega_o}{c} - \frac{1}{2} \frac{\vec{q}_o}{\frac{n_o \omega_o}{c}}. \tag{2.21}$$

Morever because $\nu_j \ll \Omega_j$ we expand the first term of second member and obtain

$$k_{oz} = K_o + \frac{\nu_o}{u_o} - \frac{|\vec{q}_o|^2}{2K_o}. \tag{2.22}$$

With similar calculations one can show that

$$k_{ez} = K_e + \frac{\nu_e}{u_e} - \frac{|\vec{q}_e|^2}{2K_e} - q_{ex} N, \tag{2.23}$$

where

$$N = \frac{\partial \left(\log \left[n_e \left(\Omega_e, \Psi_{OA} \right) \right] \right)}{\partial \Psi_O A}. \tag{2.24}$$

Note that (2.24) depends on the variation of n_e with Ψ_{OA}, so the mis-match function will ultimately depend on the optic axis direction. Finally the mis-match function becomes

$$\Delta = \nu D - \frac{N^2 \bar{K}}{4} + \frac{1}{\bar{K}} \left(\vec{q}_e + \frac{N \bar{K}}{2} \hat{u}_x \right)^2 \tag{2.25}$$

$$\frac{1}{\bar{K}} = \frac{1}{2} \left(\frac{1}{K_o} + \frac{1}{K_e} \right) \tag{2.26}$$

$$D = \frac{1}{u_o} + \frac{1}{u_e}. \tag{2.27}$$

To understand the meaning of our results we look for the zero condition of Δ. We get the circonference equation

$$\bar{K} \frac{N^2 \bar{K}}{4} - \nu D = \left(\vec{q}_e + \frac{N \bar{K}}{2} \hat{u}_x \right)^2. \tag{2.28}$$

We then can see that the extraordinary photon will lie on a circle on the x-y plane, with radius and center given by

$$R = \sqrt{\frac{N^2 \bar{K}^2}{4} - \nu D K} \tag{2.29}$$

$$C = -\frac{N \bar{K}}{2} \hat{u}_x \tag{2.30}$$

It is easy to show that similar equations hold for the ordinary photon. As a consequence we get two circles, shifted each other and crossing in two points, where polarization entangled photons are generated. In fact, if the incoming photon is in the state $|H\rangle$, in the intersections

we will find $|H\rangle$ and $|V\rangle$ polarized photons. However it is not possible to know where we will find $|H\rangle$ or $|V\rangle$ untill we measure photons' polarization. Hence with BBO, through SPDC process, we have generated the polarization entangled state

$$|\Psi^{\pm}\rangle = \frac{1}{\sqrt{2}}\left(|H\rangle_A|V\rangle_B \pm |V\rangle_A|H\rangle_B\right), \tag{2.31}$$

where A and B are the crossing point between $|H\rangle$ and $|V\rangle$ circles.

Second Harmonic Generation

Now we describe SHG process. Consider an entering beam which splits in two beams. One beam will have the same frequency of the entering beam, while the second one will have double frequency. This follows from crystal's **non-linearity** that can be expressed by

$$\vec{P} = \epsilon_0\left(\chi_{(1)}\vec{E} + \chi_{(2)}\vec{E}^2 + ... + \chi_{(j)}\vec{E}^j\right). \tag{2.32}$$

Consider the optical field dependent on time and position

$$\vec{E}(\vec{r},t) = E_0 e^{i\omega t} + E_0^* e^{-i\omega t}, \tag{2.33}$$

where $E_0^{(\pm)}$ are space dependent. Suppose that in (2.32) we have only the quadratic term and calculate polarization. We get

$$\vec{P}(\vec{r},t) = \epsilon_0\left[\chi_{(2)}\left(2|\vec{E}|^2 + E_0^2 e^{i2\omega t} + E_0^{*2} e^{-i2\omega t}\right)\right]. \tag{2.34}$$

We note that, beside the constant term, a term with double frequency is present. Thus a beam entering an SHG term will double its frequency. It is worth observing that because of non perfect efficiency, after SHG crystal one will observe both original and doubled frequency's beams.

2.3 Generation of Hyper-entangled states

In this experiment we aim to generate a time-polarization hyper-entangled state that will have the general form

$$|\Xi\rangle = \frac{1}{2}\left(|S\rangle_A|S\rangle_B + e^{i\theta}|L\rangle_A|L\rangle_B\right)\otimes\left(|H\rangle_A|V\rangle_B + e^{i\eta}|V\rangle_A|H\rangle_B\right). \tag{2.35}$$

In this section we will enter some details about the way in which hyper-entangled photons are generated.

Laser source. We use a pulsed laser source, *Mira-HP* $Coherent^{\circledR}$, with the features in Tab. (2.1), which exploits mode locking process to generate pulses.

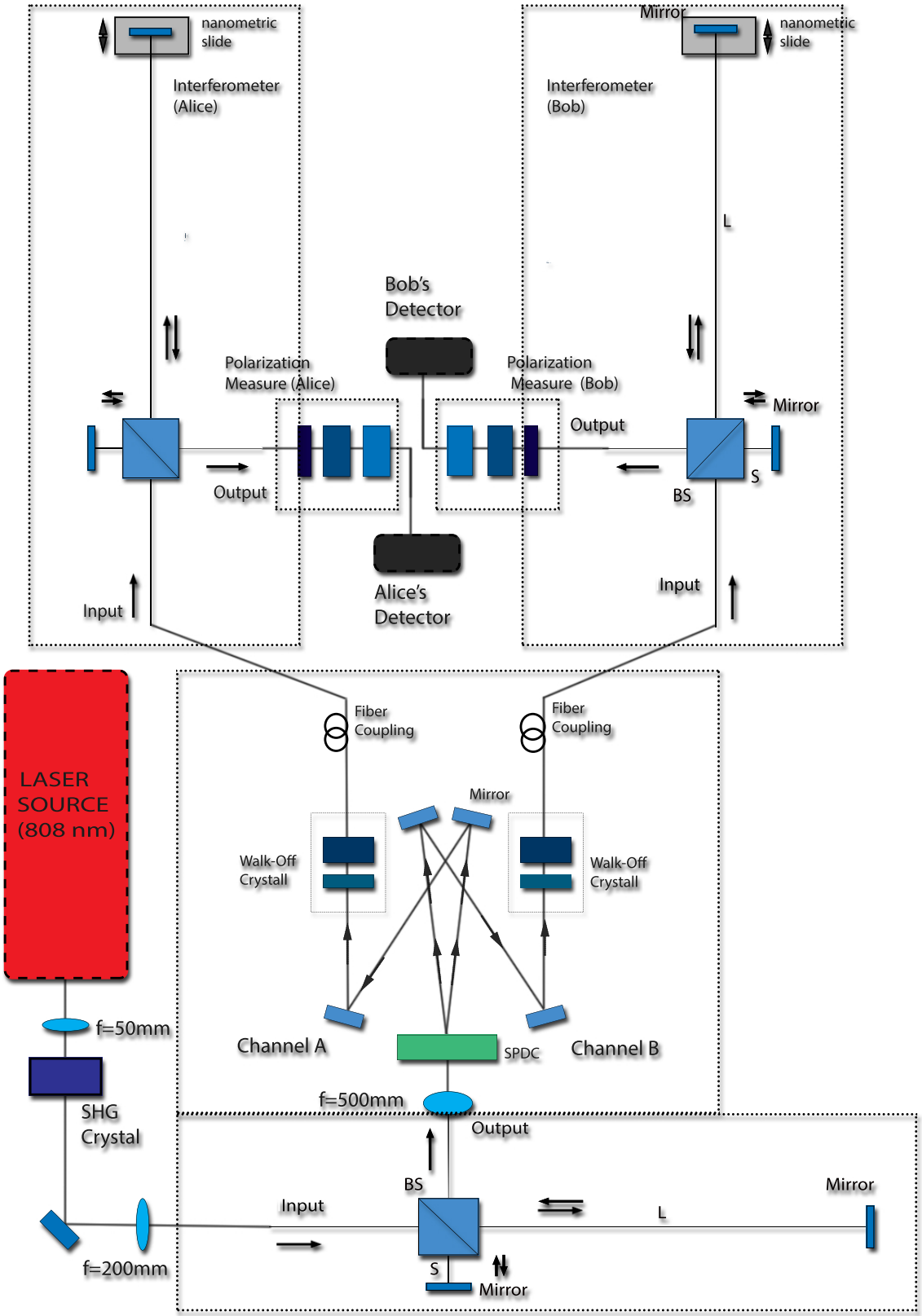

Figure 2.2: Here we show a scheme of the complete apparatus; in this chapter we explain generation and measurement processes, both present in this scheme.

Wavelength	808 nm
Power	$\sim$ 3,2 W
Pulses Rate	76 MHz
Pulse Width	130 fs

Table 2.1: Properties of source laser.

Second Harmonic Generation. Pulses are then focused with a 50 mm focal length lens at a **Bibo** crystal which makes Second Harmonic Generation by which we obtain 404 nm photons. Focalization is needed because SHG efficiency is given by

$$\eta_{SHG} \sim \frac{L^2}{A} P, \tag{2.36}$$

where L is the crystal length, A the crystal's section intersected by the beam and P the beam power. We note that, fixed L, efficiency will grow up with P and decrease with A. SHG efficiency is found to be about $\eta_{SHG} = 37\%$.

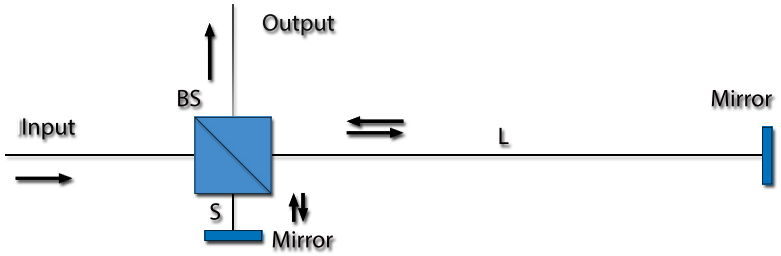

Figure 2.3: Scheme of a Michelson's unbalanced interferometer. We can see a great difference between long and short arm. This guarantees that no single photon interference will occur.

Time entanglement generation. After SHG crystal we put a f=200 mm lens to collimate our beam. This is necessary if we want to propagate the beam on free space. As long as we want to have time entangled states we must generate some indetermination on single pulses' position. In fact, until now it would be always possible to determine with high precision pulses' position by checking when they exit the Bibo crystal and calculating the time they need to get the measurement position. To "generate indetermination" we use a **Michelson interferometer**

(Fig.2.3). What we need is an unbalanced interferometer, such that the paths' difference is greater than the coherence length of single photons, because we want to avoid single photons interference. In general, after the interferometer, we have the single photon state

$$|\tau\rangle = \frac{1}{\sqrt{2}}\left(|S\rangle + e^{i\theta}|L\rangle\right), \tag{2.37}$$

where $|S\rangle$ and $|L\rangle$ label the short and long arm respectively.

BBO: Hyper-Entanglement state Generation. Photons that are in the state (2.37), are focused at the BBO crystal with a f=500 mm lens. Again focalization allows to increase pair production by SPDC process. BBO is perhaps the central tool in our experiment. It allows *Spontaneous Parametric Down Conversion* (SPDC) process. SPDC splits the incoming photon in two photons, so, in general, we obtain the state

$$|\tau\rangle = \frac{1}{\sqrt{2}}\left(|S\rangle_A|S\rangle_B + e^{i\theta}|L\rangle_A|L\rangle_B\right). \tag{2.38}$$

Moreover the photons generated by SPDC are entangled in different degrees of freedom. Among the different DOFs we take advantage of polarization. Taking the intersections of fig. (2.1) between ordinary and extraordinary photons we get H and V polarized photons. Nevertheless we do not know, before measurements, which photon will be H and which one will be V. Thus we have polarization entanglement which sum with (3.17), and we obtain

$$|\Xi\rangle = \frac{1}{2}\left(|S\rangle_A|S\rangle_B + e^{i\theta}|L\rangle_A|L\rangle_B\right) \otimes \left(|H\rangle_A|V\rangle_B + e^{i\eta}|V\rangle_A|H\rangle_B\right). \tag{2.39}$$

Walk-off crystal. Because of birefringence effects due to different polarizations of the generated photons, we will observe the $|V\rangle$ photon before $|H\rangle$ photon. This could be a problem because it allows to distinguish the different polarization states. To get over this difficulty we insert, after SPDC, on both channels, a $\lambda/2$ wave plate and a *Walk-Off Crystal*. This is nothing but a birefringent BBO crystal in which $|V\rangle$ has a greater velocity than $|H\rangle$, and it is chosen so that, after it, photons are in the same position, along each path. Figure (3.1) will help us to understand this operation. We have seen that with walk-off crystals we are able to modify phase difference between the photons. This means that we are also able fix $\eta = 0, \pi$ to obtain $|\Psi^+\rangle$ or $|\Psi^-\rangle$. In our work we will check both $|\Psi^+\rangle$ and $|\Psi^-\rangle$, passing from one state the other simply rotating walk-off crystal's optical axis, and the experimental results will refer to $|\Psi^-\rangle$ state.

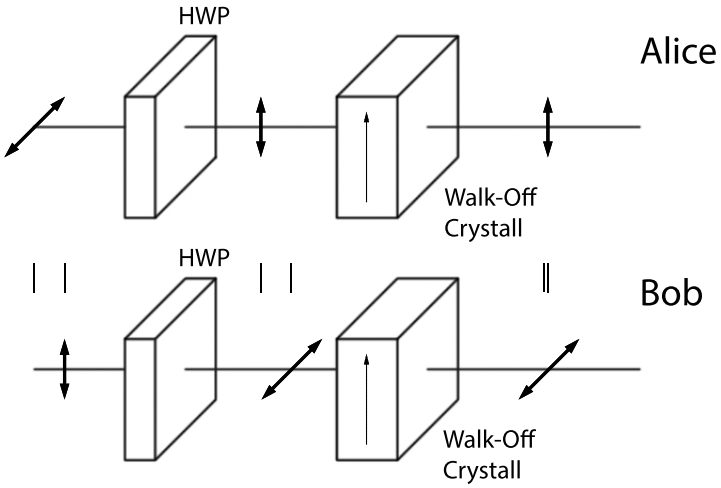

Figure 2.4: Correction obtained with Walk-Off Crystals. We note that if we would invert polarization in channel A and B we would get the same result.

Chapter 3

Hyper-entangled photons Measurements

In this chapter we are going to describe the measurements process for hyper-entangled states. At first we concentrate on single DOF's measurements, describing the basic theoretical ideas connected with this goal. The hyper-entanglement measure is nothing but the simoultaneous measure of both time-bin and polarization. Then we will face with some issues related with the way in which we process our raw data. We will describe the method to recover the coincidences, letting to the last section some theoretical aspects about the quantum density matrix and the methods used to recover it starting from experimental coincidences. After this we will describe the *synchronization* technique, that will play a central role in this experiment. The last part of this chapter will deal with quantum density matrices and the methods used to recover them.

3.1 Measurement process

Here we describe the theory and the central ideas useful to measure time and polarization states. Beside pratical differences, due to different experimental tools, we will observe some similarities between time and polarization observables. This fact allows us to treat them in a similar way. This implies that we will be able to observe Bell's inequality violation in both cases, and density matrices for time and polarization will have almost the same form.

3.1.1 Polarization Measurement

When treating polarization states it is useful to introduce *Jones Calculus*, which allows us to work with 2x2 matrices, easy to calculate. Jones Calculus represents polarization eigenstates as vectors on Hilbert space $\mathcal{H} \approx \mathbb{C}^2$:

$$|H\rangle \equiv \begin{pmatrix} 1 \\ 0 \end{pmatrix}; \qquad |V\rangle \equiv \begin{pmatrix} 0 \\ 1 \end{pmatrix}, \tag{3.1}$$

such that $|\Psi^{\pm}\rangle$ can be written as

$$|\Psi^{\pm}\rangle = \frac{1}{\sqrt{2}}\left[\begin{pmatrix} 1 \\ 0 \end{pmatrix}_A \begin{pmatrix} 0 \\ 1 \end{pmatrix}_B \pm \begin{pmatrix} 0 \\ 1 \end{pmatrix}_A \begin{pmatrix} 1 \\ 0 \end{pmatrix}_B\right]. \tag{3.2}$$

When treating polarization states we take advantage of *wave retarders* and *polarizing beam splitters* to manipulate polarization states.
Wave retarders are birefringent plates with different refractive indexes associated to different directions. Hence *ordinary* component of electric field will have greater group velocity than the *extraordinary* one. This implies that a phase difference between o and e components is generated inside the plate:

$$\Delta\phi = \frac{2\pi}{\lambda}(n_o - n_e)L. \tag{3.3}$$

In (3.3), n_e and n_o are the refractive indexes and L is the plate width. Two particular cases are

- $\lambda/4$ wave plates where $(n_o - n_e)L$ is odd multiple of $\lambda/4$ in which the outcoming phase difference will be $\pi/2$. These plates can be used to transform linear polarization states into circular polarization ones.

- $\lambda/2$ wave plates where $(n_o - n_e)L$ is odd multiple of $\lambda/2$ in which the outcoming phase difference will be π. These plates can be used to rotate polarization state.

Wave retarders with vertical optical axis can be represented by

$$P_{\lambda/4} \equiv \begin{pmatrix} 1 & 0 \\ 0 & -i \end{pmatrix}, \tag{3.4}$$

$$P_{\lambda/2} \equiv \begin{pmatrix} 1 & 0 \\ 0 & -1 \end{pmatrix}. \tag{3.5}$$

Considering the rotation operator

$$R(\theta) = \begin{pmatrix} \cos\theta & -\sin\theta \\ \sin\theta & \cos\theta \end{pmatrix}, \tag{3.6}$$

we can write the rotation of wave retarders as

$$P_{\lambda/4}(\theta) = R^{-1}(\theta)P_{\lambda/4}R(\theta) = \begin{pmatrix} \cos^2\theta - i\sin^2\theta & (-1-i)\sin\theta\cos\theta \\ (-1-i)\sin\theta\cos\theta & \sin^2\theta - i\cos^2\theta \end{pmatrix} \tag{3.7}$$

and

$$P_{\lambda/2}(\theta) = R^{-1}(\theta)P_{\lambda/2}R(\theta) = \begin{pmatrix} \cos 2\theta & -\sin 2\theta \\ -\sin 2\theta & -\cos 2\theta \end{pmatrix}. \tag{3.8}$$

Polarizing beam splitters (PBS) are beam splitters where the transmitted wave has a defined polarization and the reflected one has the orthogonal polarization. One immediately finds that vertical and horizontal oriented PBS can be expressed as projection operators

$$P_H \equiv |H\rangle\langle H| \equiv \begin{pmatrix} 1 & 0 \\ 0 & 0 \end{pmatrix}, \tag{3.9}$$

$$P_V \equiv |V\rangle\langle V| \equiv \begin{pmatrix} 0 & 0 \\ 0 & 1 \end{pmatrix}. \tag{3.10}$$

Now we calculate again (1.7). In this case we substitute spin-up and spin-down eigenstates with H and V eigenstates and we use polarization eigenstate projectors instead of pauli measurements. We show that this way we can approach Bell's test with polarization states photons, more suitable for experiments than spin measurements. We calculate the coincidences rates with photons' polarization rotated of angles α_P and β_P where the rotation is obtained with the aid of $\lambda/2$ wave plates. Considering $|\Psi^{\pm}\rangle$ state, we operate a rotation and a projection on the vertical axis. The states are

$$\begin{aligned} |\Psi_{\alpha_P,\beta_P}\rangle \equiv & \begin{pmatrix} 0 & 0 \\ 0 & 1 \end{pmatrix} \begin{pmatrix} \cos 2\alpha_P & -\sin 2\alpha_P \\ -\sin 2\alpha_P & -\cos 2\alpha_P \end{pmatrix} \\ & \begin{pmatrix} \cos 2\beta_P & -\sin 2\beta_P \\ -\sin 2\beta_P & -\cos 2\beta_P \end{pmatrix} |\Psi^{\pm}\rangle \end{aligned} \tag{3.11}$$

$$= \frac{1}{\sqrt{2}} \left[\cos 2\alpha_P \cos 2\beta_P \mp \sin 2\alpha_P \sin 2\beta_P\right] |V\rangle_A |V\rangle_B. \tag{3.12}$$

For " $+$ " choice the amplitude is defined as

$$A_P(\alpha_P, \beta_P) = \frac{1}{\sqrt{2}} \left[\sin 2\alpha_P \sin 2\beta_P + \cos 2\alpha_P \cos 2\beta_P\right] \tag{3.13}$$

$$= \frac{1}{\sqrt{2}} \left[\sin(2\alpha_P + 2\beta_P)\right], \tag{3.14}$$

hence finally we get the coincidences rate for polarization state

$$C_P(\alpha_P, \beta_P) \equiv |A_P(\alpha_P, \beta_P)|^2 \tag{3.15}$$

$$= \frac{1}{2} \left[\sin^2(2\alpha_P + 2\beta_P)\right]. \tag{3.16}$$

We thus have obtained the same result of (1.9), showing that it is possible to make Bell's type experiment with polarization DOF. Experiments on polarization entanglement have been done first by Aspect et al. in 1981 and 1982 [4].

3.1.2 Time measurement

At this stage we want to measure time entangled state

$$|\tau\rangle = \frac{1}{\sqrt{2}} \left(|S\rangle_A |S\rangle_B + e^{i\theta} |L\rangle_A |L\rangle_B\right). \tag{3.17}$$

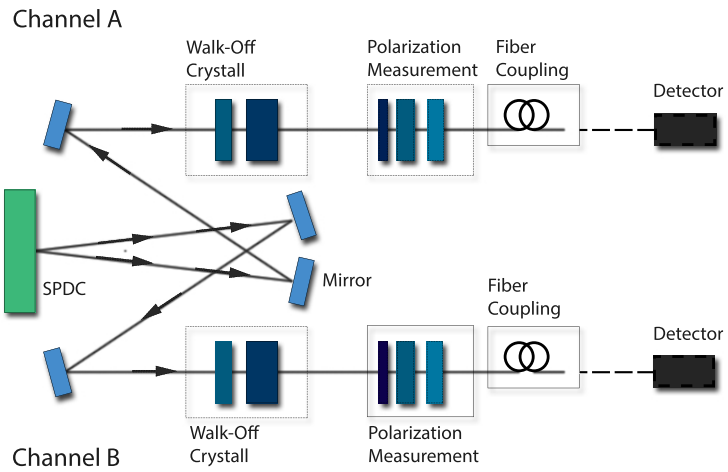

Figure 3.1: Here we represent SPDC and polarization measurement set up. This is all one needs to perform Bell's measurement or quantum tomography exploiting polarization states.

What we need is two unbalanced Michelson inteferometers similar to that described above. We calculate the coincidence probability between the interferometers. From (3.17) the entanglement for a single pair can be generated in two different moments, depending on the path chosen by the pump photons in the pump interferometer. Moreover both cases the outcome will be

$$\begin{aligned} |\tau_A\rangle &= \frac{1}{\sqrt{2}}\left(|S\rangle_A + e^{i(\alpha_\tau+\theta)}|L\rangle_A\right) \\ |\tau_B\rangle &= \frac{1}{\sqrt{2}}\left(|S\rangle_B + e^{i(\beta_\tau+\theta)}|L\rangle_B\right), \end{aligned} \tag{3.18}$$

where β_τ and α_τ are relative phases between long and short arms. Here we observe that such outcomes entail that the interferometers operate a projection described (for A channel) by

$$P_{\tau_A} = \frac{1}{\sqrt{2}}\left(|S\rangle_A + e^{i\alpha_\tau}|L\rangle_A\right)\left(\langle S|_A + e^{-i\alpha_\tau}\langle L|_A\right). \tag{3.19}$$

This is formally the same operator that describes polarization projection. To find out the coincidence probability we must project one of (3.18) on the other and take the square modulus.

$$\begin{aligned} C_\tau(\alpha,\beta) \equiv |A(\alpha,\beta)|^2 &\equiv |\langle\tau_B|\tau_A\rangle|^2 \\ &= \frac{1}{4}|1+e^{i(\alpha_\tau-\beta_\tau)}|^2 \\ &= \frac{1}{2}\left[1+\cos(\alpha_\tau-\beta_\tau)\right] \equiv \left[\cos^2(\frac{\alpha_\tau-\beta_\tau}{2})\right]. \end{aligned} \tag{3.20}$$

We note that we have obtained a similar coincidence equation to that of polarization entanglement. This fact suggests that time measurements can be done as polarization ones, where relative phases are obtained by varying long arms' length instead of rotating wave plates.

3.1.3 Hyper-entanglement measurement

Until now we have described how to measure polarization and time separately. To measure hyper-entangled states it will suffice to put A and B polarization measurement stage after each interferometer (or vice versa) and detect photons after the complete measurement's set up.

3.2 Coincidences

Summing up, to measure polarization states we project the generated photons on that state with the help of wave retarders and the polarazing beam splitters. To measure time states we move forth and back the nanometric slides to change the phase in the interferometers or we project the single photons' state on $|L\rangle$ or $|S\rangle$ eigenstates by closing the proper arm with the help of two shutters. After this we collect the exiting photons with two Single Photon Avalanche Photodiodes (SPAD). For each revealed photons they send a square pulse that is registred on a Time to Digital Converter (TDC), $QuTau^{®}$. Our TDC has many BNC ports and in this case we use the first and the second to collect channel A and B respectively.

Figure 3.2: Here the TDC. We observe 8 ports, and we use three of them. One for signals from photons in channel A, one for signals from photons in channel B and the third one for trigger signals

To process our data we have to fix a time reference. To do so we take part of a pulsed signal exiting the SHG. This signal is detected by a photo-diode that produces a 76 Mhz analogic signal that is registred in the third port of the $QuTau^{®}$. Then the Qutau will register:

- On the first channel, signals coming from photons on channel A;
- On the second channel, signals coming from photons on the channel B;
- On the third channel, trigger signals that provide a time reference.

For this reason we will have an array similar to that reported in (3.1). Now we have to find a criterion for which events on A and B channels can be considered events due to entangled

t_1	t_2	...																				t_n
B	A	B	T	T	B	A	T	T	B	A	T	T	B	A	T	A	B	T	B	A	A	T

Table 3.1: Sample from a string recovered after the synchronization. On the first row arrivals' time is labelled, while on the second row arrivals are registred. T is the trigger signal, A and B are signal photons revealed on channel A and B respectively.

photons. To do this we fix a coincidence window and look for A and B events that both fall on the same window.

For each channel A and B we can refer the time arrival of a signal photons to the trigger signal. Because of this, performing the module operation, we can understand what path the photons chose. The time arrivals depend on the path choosen for the pump photons.
In figure (3.3) we observe the photons time arrivals for channel A and B.

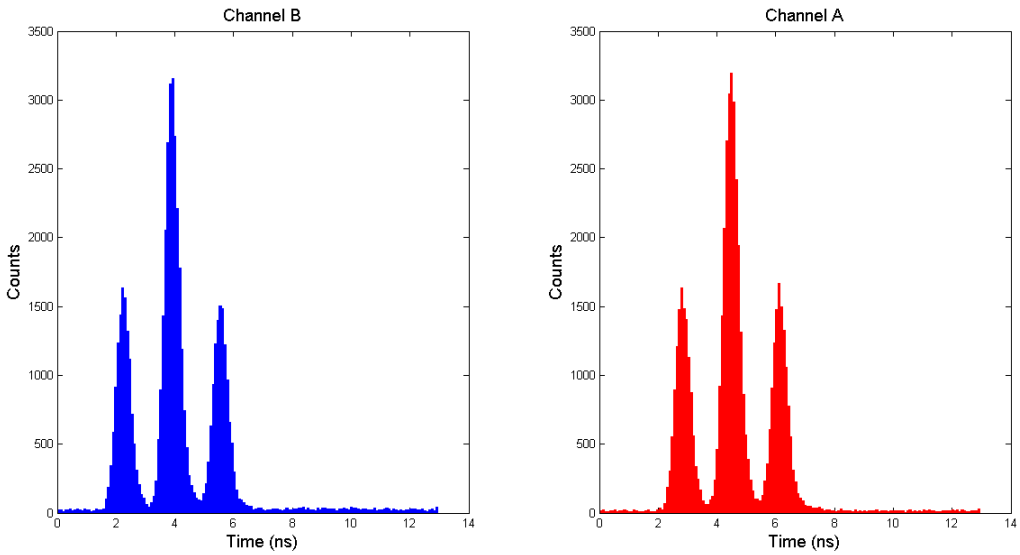

Figure 3.3: Here the histograms of time arrivals. We observe three peaks correnspondingto the different path along the pump interferometer and the measurement interferometer. We report the data with a window of 13 ns for the module operation. This is because the original signal was a 76 Mhz pulsed one.

In figure (3.4) we observe together the singles of both channels. A corrected delay of 25 ns is present. Until now we have considered the A and B channel as separated, and we have not looked for the coincidences yet. Now we have to look at the subset of singles in which entangled photons could be found. It is important to remember that the entanglement is characterized by indistiguishable states. To understand the situation we can look at figure (3.5). The entangled photons are the black dots inside the circle. In fact, in that case we do not know if the pump photon chose the short/long path. As a consequence, for those photons we

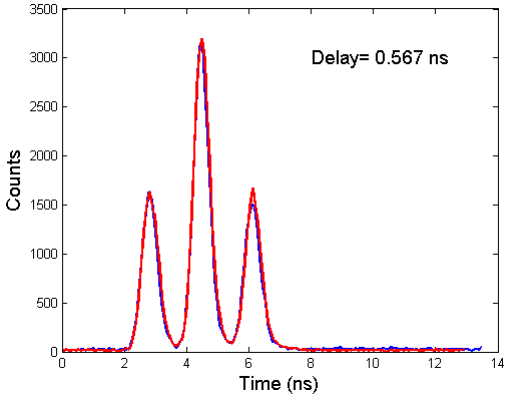

Figure 3.4: Here the histograms of time arrivals together in the same graphic. A 25 ns delay is corrected via software. This is necessary in order ot recover the coincidences

do not know when they were generated. In particular, for the black dots, we do not know if the pump photon chose the long arm and the entangled photons chose the short one, or vice versa. Then because of this indistinguishable possibilities, we have the entangled pair.
This is the time-entangled state

$$|\tau\rangle = \frac{1}{\sqrt{2}}\left(|S\rangle_A|S\rangle_B + e^{i\theta}|L\rangle_A|L\rangle_B\right). \tag{3.21}$$

Now we have to characterize the coincidence window that should contain any pair in the central peak. For this reason we put a low and up threshold, that allow us to consider just the singles in the central peak. No entangled pair should have photons from the first and last peaks. As a second step we have to think about our physical system. Because of conservation laws, the entangled photons should be generated at the same time. Taking into account the accuracy of our instruments we fix a coincidence window of 12 bins, that correnspond to 1 ns. All pairs that will be found within a time window of 12 bins will be considered entangled photons. In fig. (3.6) we observe an example of what we obtain: three peaks of correlated photons. The first and third peaks are not due to entangled photons because we know the state that generated these peaks. For the first peak it was $|S\rangle|S\rangle$ while for the third peak it was $|L\rangle|L\rangle$. These are obviously separable states.

We will use this method to determine the counts of hyper-entangled photons for all the data we will acquire. We now observe that there will be also different situations from that described above. When performing a quantum tomography, for example, we will project a single photon on the state $|L\rangle$. Obviously no single photon will be found in the first peak. Two extreme possible situations could be observed. In the first case we could project our time-entangled state on the state $|L\rangle|L\rangle$, as fig. (3.7) shows.

In the second case we could project our time-entangled state on the state $|S\rangle|L\rangle$, as fig. (3.8) shows. In that case no coincidence will be observed, because the photons will not be indistinguishable anymore.

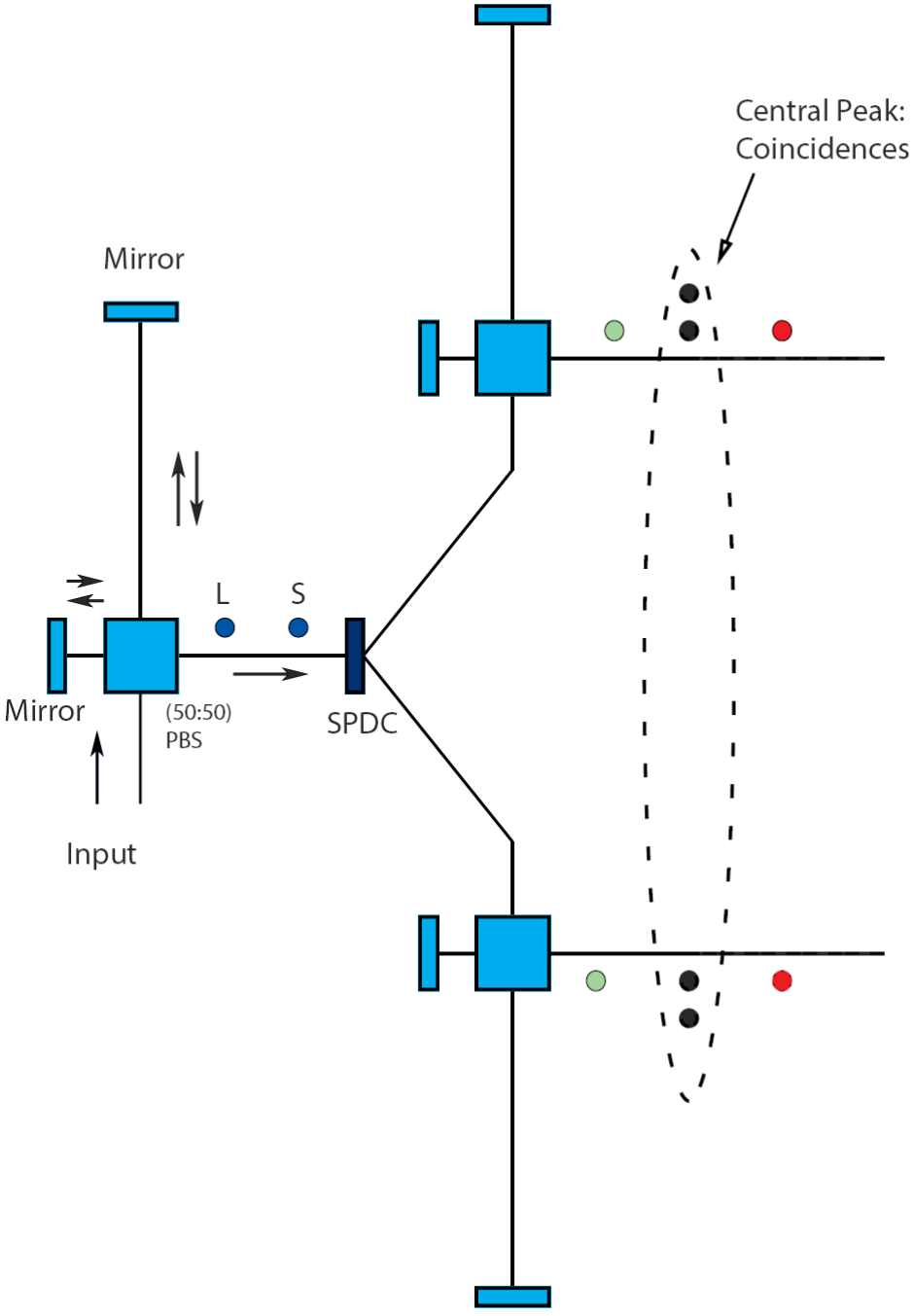

Figure 3.5: The pump photons can run the long or short path. This entails that the entangled pairs could be generated in two different moments, this is why we observe two dots labelled as S and L. In the interferometers in which we perform our measures, the photons can choose the long or short path. The entanglement his related with those photons for which we cannot know when they were generated, that are the black circled pairs. Note that for the red pair we are certain that the pump photon chose the short path and that they were generated before. For the green pair we are certain that the pump photon chose the long path. In these case no superposition is present and as a consequence the photons are not entagled

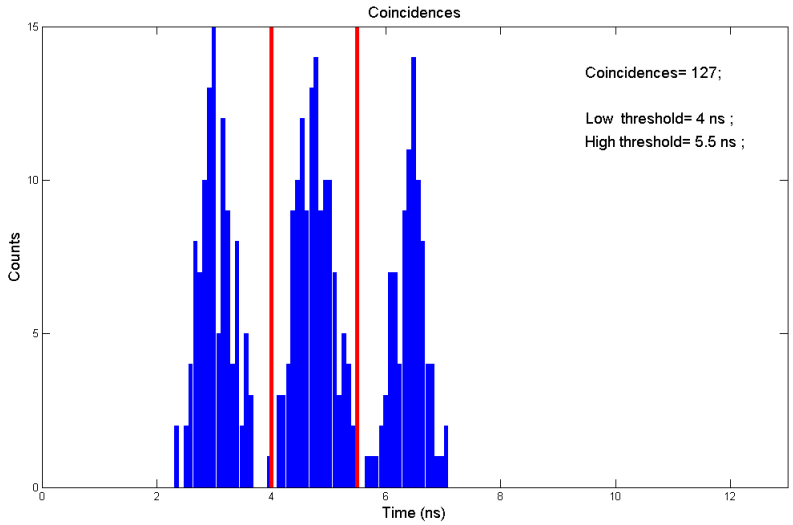

Figure 3.6: Here the histograms of time arrivals together in the same graphic. A 25 ns delay is corrected via software. This is necessary in order ot recover the coincidences

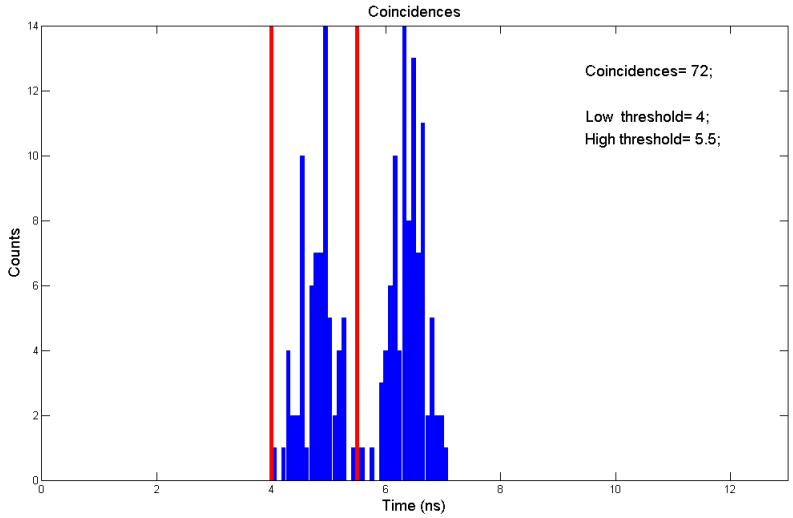

Figure 3.7: Here we project both photons A and B on the $|L\rangle$ eigenstate

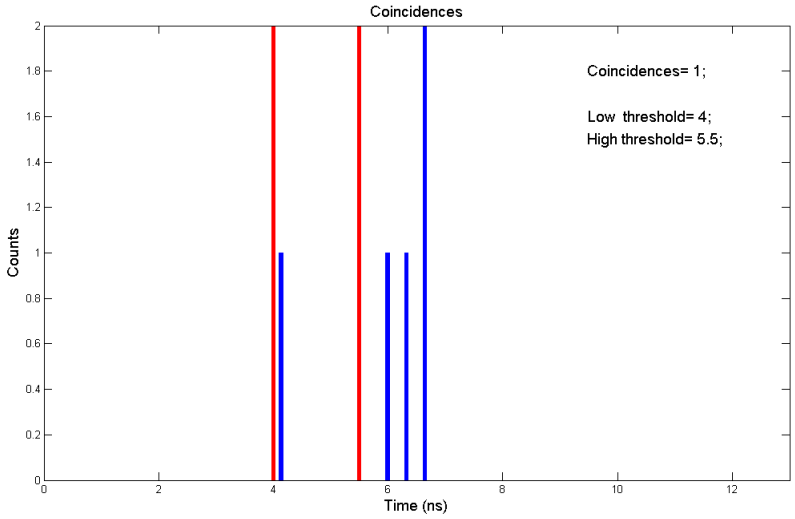

Figure 3.8: Here we project both photons B on the $|L\rangle$ eigenstate and A on the $|S\rangle$ eigenstate. No pair and thus no coincidence will be found inside the coincidence window in the central peak.

Interference

In this part we describe some observations related with time entanglement measures. In our experiment variation of long's arm length is obtained with two $Smaract^{®}$ nanometric slides, that allow us to work on single photons' phases with a good precision. We observe that some conditions have to be satisfied:

$$D = L - S \gg l_{coh} \tag{3.22}$$

$$D_L = |(L_A - S_A) - (L_B - S_B)| < l_{coh}. \tag{3.23}$$

$$D_{L1} = |(L_{A(B)} - S_{A(B)}) - (L - S)| < l_{coh}. \tag{3.24}$$

Here l_{coh} is the coherence length defined as $l_{coh} \equiv c\tau_{coh}$. For pulsed sources, the coherence time is ultimately associated to single pulses duration. (3.22) guarantees that no single photon interference will occur. This condition is immediately verified by observing that, in our set up, D is about 30 centimeters while the coherence time is a fraction of a picosecond and as a consequence the coherence length will be on the order of hundreds microseconds. The second condition puts some limits on the length difference between A and B interferometers' long arms. In this case we check (3.23) by varying D_L with a relative long step and observing that an interference pattern grows up while getting close to $D_L = 0$. Before beginning our measurements we checked that this interference pattern was centered around the zero value for each slide. This fact would have implied that condition (3.24) was satisfied. To do so we moved one of the two slides with 3 μm step letting the second one in a fixed position. In this way we were able to plot an interference pattern such that in figure (3.9). In this figure we

observe a growing interference around the zero value. Moreover, with this figure, we are able to estimate the coherence length for the photons. In fact, over the coherence length we will not observe interference anymore, as happens in figure (3.9) over $\sim \pm 80 \mu m$. Even though this is not to be considered a precise measure, it helps us to understand the coherence length's order of magnitude. Another important step when measuring time entanglement is to estimate the

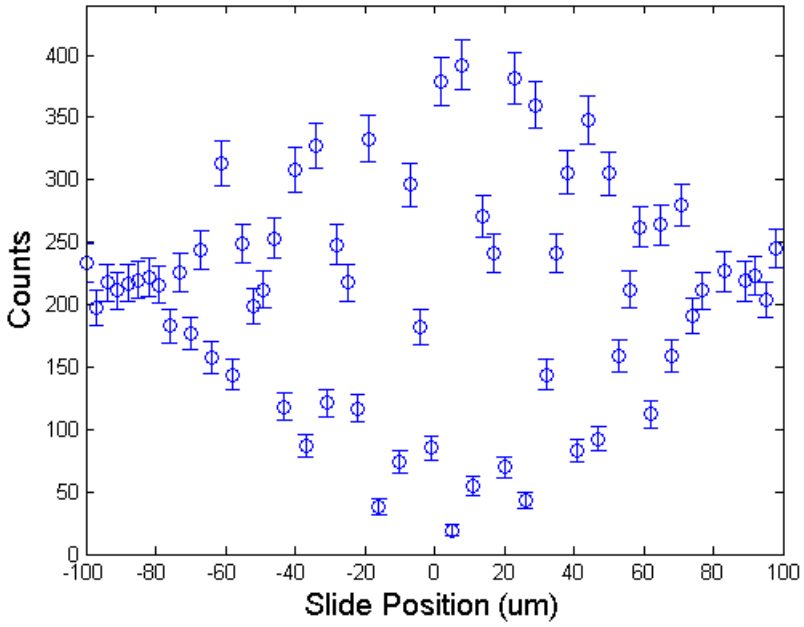

Figure 3.9: Here we report the interference pattern when moving one of the two slides by a 3 μm step over a 200 μm range. We observe maximum interference at zero and vanishing interference over ± 80 μm.

visibility of the state, defined as

$$\mathcal{V} = \frac{C_{Max} - C_{Min}}{C_{Max} + C_{Min}}, \tag{3.25}$$

where C_{max} and C_{min} label the maximum and mininum for the interference pattern in (3.10) A rapid look at figure (3.10), allows to observe that $\mathcal{V} \geq 95\%$. Moreover looking at the distance between two following maxima(minima), this distance is observed to be $\sim$400 nm. This is nothing but the wavelength of our pulsed laser. Then, thanks to these two graphics we are able to extract a great amount of information about our interferometers and our system in general.

Stability

However, some problems arise when working at such a high precision. In fact, because we need to work on the photons' phase, we have to be precise at the order of some nanometers.

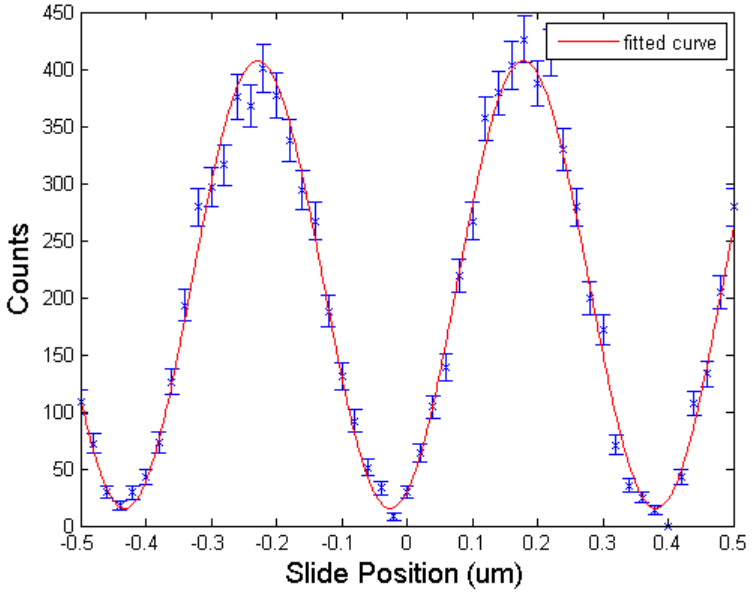

Figure 3.10: Here we report the interference pattern when moving one of the two slides by a 0.02 μm step over a 1 μm range. A regular sinusoidal pattern, as expected by the previous formulas.

A wrong slides' position would imply a wrong phase. As a consequence we will measure a different state from that we wanted to measure. This problem is important in particular for those measures of interference. Here we make an important observation: we can divide our possible measures into two groups. The first group is characterized by one or both interferometers in which the long or short arms are closed. In that case, as one can see with simple calculations, no interference will appear. Thus if there are closed arms, there is no need to fix the slide position with great accuracy. The second group is characterized by both open arms in the interferometers. The problem of stability is connected to this group of measurements.
To explain the problem we make a simple calculation. Suppose we want to project our time entangled state on the state $|D\rangle_A|R\rangle_B$. We write these states as functions of $|S\rangle$ and $|L\rangle$ eigenstates, and project one on the other

$$|\langle D|R\rangle|^2 \equiv \frac{1}{2}|(\langle S| + \langle L|)(|S\rangle + e^{-i\frac{\pi}{2}}|L\rangle)|^2 \tag{3.26}$$

$$= \cos^2\frac{\pi}{4} = \frac{1}{2}. \tag{3.27}$$

Now we write the phase as a function of the slide's movement

$$|\langle D|R\rangle|^2_{exp} = \cos^2\left[\left(\frac{\pi}{404\ nm}\right)(101\ nm)\right]. \tag{3.28}$$

At this point we can estimate how a wrong movement can influence the resulting counts. If we consider a 10 nm error, for example, we have to substitute 101 nm with 91 nm (or 111) nm,

obtaining 0.58 and 0.42. Thus, small errors on the slide's movement can influence our measure by more than a 10 $\%$. Unfortunately it happens that the environment provokes even larger movements on the slides. Small vibrations, as well as slight temperature gradients become a problem. A solution is an active control which exploits the laser itself. Before each measure in which both arms are open, we move one slide with 80 nm steps along a couple of wavelength periods. An interference figure similar to (3.10) is then plotted. We then look for the minimum in the interference pattern and choose that point as the starting point from where we move the slides. This is possible because as one can seen in (3.17) there is a free phase θ to be fixed. This method allows us to have a fixed reference phase from which we move forth or back to obtain the wanted measurement positions. It is worth noting that this choice entails that our time entangled state will become

$$|\tau\rangle = \frac{1}{\sqrt{2}} \left(|S\rangle_A |S\rangle_B - |L\rangle_A |L\rangle_B \right). \tag{3.29}$$

Thus, the hyper-entangled state in the most general case was described as

$$|\Xi\rangle = \frac{1}{2} \left(|S\rangle_A |S\rangle_B + e^{i\theta} |L\rangle_A |L\rangle_B \right) \otimes \left(|H\rangle_A |V\rangle_B + e^{i\eta} |V\rangle_A |H\rangle_B \right). \tag{3.30}$$

Thanks to the stability process and the proper rotation of the walk-off crystals we obtain the specific state

$$|\Xi\rangle = \frac{1}{2} \left(|S\rangle_A |S\rangle_B - |L\rangle_A |L\rangle_B \right) \otimes \left(|H\rangle_A |V\rangle_B - |V\rangle_A |H\rangle_B \right). \tag{3.31}$$

3.2.1 Synchronization

Until now we have considered to work with a single terminal in which we use two different BNC channels to collect photons from channel A and channel B on a sigle Time to Digital Converter. In this way we have avoided some problems related with the fact that, if we want to perform free-space quantum communications, our terminals will be separated in space and indipendent.

Now we will provide a technique that allows us to synchronize indipendent TDC to recover hyper-entangled photons measure in distant terminals. For each channel the set up is the following. After the measurement stage we put a single photon avalanche photo-diode (**SPAD**) which exits a TTL signal for each single revealed photon. The signal is sent to a Time to Digital Converter module, $QuTau^{\circledR}$, that registers time arrival for each photon. The difference between this set up and that one described in section 3.6 is that now we have two separated TDCs, one for each channel A and B.

In the meanwhile, at the output of laser, that in our case is Alice's position, the beam after exiting the SHG crystal is used as a **trigger signal**. It is sent to Alice's photo-diode (PD), which exits an analogic signal that is decimated through a FPGA and divided into two trigger signals. The decimation allows to reduce the pulses frequency from a 76 Mhz to a 5 Khz

signal. The first signal is recorded by Alice's TDC to provide a local reference frame, while the second one is used to estabilish an **optical link**. This optical link plays a central role as it provides a common reference frame for the parties. It is worth noting that without the optical link, it would be impossible to measure entangled states for separated parties. Moreover a sub-nanosecond accuracy is obtained with our method. This accuracy is necessary to characterize time-bin entanglement.
Now I will enter some details of the **optical link**'s mechanism. As just observed Alice is provided with a trigger signal sent to a photo-diode. The analogic signal exiting the photo-diode is divided into two signals, decimated by the FPGA. The first one, is sent to Alice's QuTau, and provides a time reference for the time of photons' arrivals at Alice's position. An example of what Qutau A will register is reported below. The second analogic signal is used to modulate

t_1^A	t_2^A	...																			t_n^A
T	A	A	T	T	A	T	A	T	A	T	A	T	T	A	A	T	A	T	T	A	T	A

Table 3.2: Sample from a string registred on QuTau. On the first row arrivals time is labelled, while on the second row is registred arrivals channel. T is the trigger signal and A is the entangled photon in the channel A.

a laser diode which emits 810 nm 5 Khz pulsed signal. Summing up, it is the pulsed diode laser that provides an optical link between Alice and Bob. In fact this optical signal is sent to a photo-diode at Bob's stage. The Bob's PD generate a square signal that is then directed to Bob's Qutau. Finally, Bob will have an array similar to that of Alice. There are some main

t_1^B	t_2^B	...																			t_n^B
B	B	B	T	T	B	T	T	T	B	T	T	T	B	B	T	T	B	T	B	B	T	T

Table 3.3: Sample from a string registred on QuTau B. On the first row arrivals time is labelled, while on the second row is registred arrivals channel. T is the trigger signal and A is the entangled photon in the channel B.

observations that are to be adressed here, related with the time arrivals on the TDCs.

- a delay between t_1^B and t_1^A will be measured. It depends on the distance between Alice and Bob and on the electronics;
- TDCs have a time unit of 81 ps, called "bin". Thus TDCs have an accuracy of about 81 ps.
- The rise time of the laser diode is 5 ns. However its slope is fixed and stable, and the standard deviation of the difference between two near pulses time arrivals is 2-3 bins.
- the TDCs, during the characteristic time of some seconds, which is the duration of a sigle measure, will drift in a different way from each other.

These four facts have to be characterized and corrected to compare Alice's and Bob's data. The method can be divided into different steps.
The fixed delay is corrected by subtracking t_1^B and t_1^A from their arrays. To do so we have to be certain that values in t_1^B and t_1^A have been originated by the same original pulse. This is achieved with a **shutter** the opens and closes the path to Alice's PD. The shutter opens rapidly and the same pulse will be registred by the parties.
The second and thirt issues imply that the registration time for pulses on the different TDCs will not be the same. We have first considered only the trigger signals at Alice and Bob's TDCs. We expected to obtain a fixed rate of 5 Khz for both TDCs, and we get two gaussian distributions around the correct mean value. Calculating the RMS of the distributions we can estimate the error in the registrations of time arrivals, as figure (3.11) shows. In that figure we can observe that the RMS is ~ 0.1 ns. This fact guarantees that we will be able to recover coincidences between channel A and B. The fourth problem is the more complex to fix and it

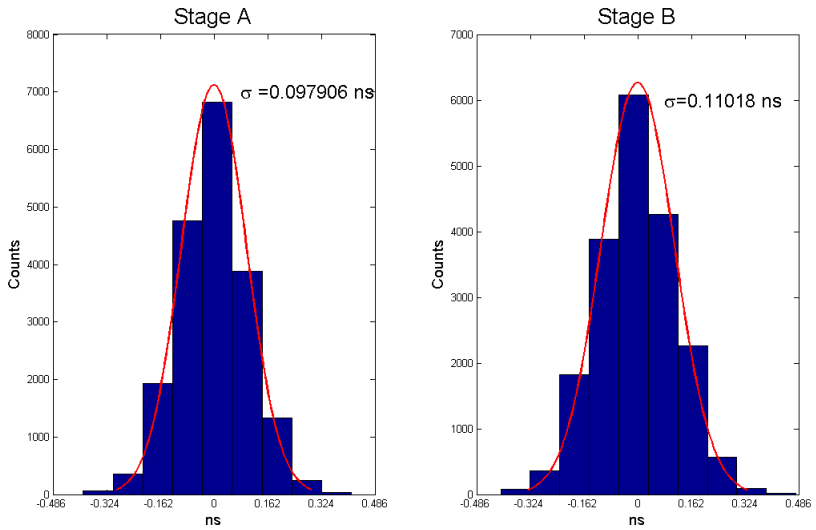

Figure 3.11: Here the histograms of differences between arrivals. We observe a gaussian distribution. A wider distribution on QuTau B is due to the rise time of the diode laser.

needs some corrections via software. Here we explain the algorithm used to correct the drift. The presence of a drift between the TDCs means that

$$t_{i+m}^B - t_i^B \neq t_{i+m}^A - t_i^A \tag{3.32}$$

for any choice of i and m. This is due to nothing but the fact that the internal clocks of the TDCs could work in a slightly different way. We have a drift between the time registrations on the different TDCs. In a few seconds the TDCs have registred a time difference of some milliseconds. Because the coincidence window, that we are going to define below, is of the order of a nanosecond, we have to solve this problem in order to correlate the parties. The

basic idea to correct this issue is the following: we divide the registred arrays into smaller slots with a characteristic time of a millisecond. Then we make the transformation given by eq. 3.33

$$t_i^B \rightarrow (t_i^B - t_0^B)\left[\frac{t_{i+m}^B - t_i^B}{t_{i+m}^A - t_i^A}\right] + t_i^A, \tag{3.33}$$

where m is the fixed dimension of a single slot, while i is the slot position on the array. Here we underline that the normalization of time registrations on B are made considering only the time arrivals of trigger signals. The time registration for photons will be corrected as a consequence of the correction on trigger signals. In this way the first and the last tag in every slot will register the same time. For the internal values of each slot, we are guaranteed that the Bob's tags will not drift away from those of Alice. In fact in the temporal range of hundreds microseconds the TDCs are stable. In figure (3.12) we show an example of a single slot of a given length. The trigger tags at stage B are registred at a different time, related with those of A. This is due to the fact that Qutau A and B works in a different way. In figure (3.13) we show the basic idea underlying the correction method. Using a Matlab script we normalize the tags in B to that tags resulted in A. In this way, even though there could be a difference between the internal trigger tags, as shown in figure, the colored tags on A and B are registred at the same time. With this method we are sure that along each measure A and B are synchronized and we are able to recover the coincidences. After this process we will obtain an array similar to that

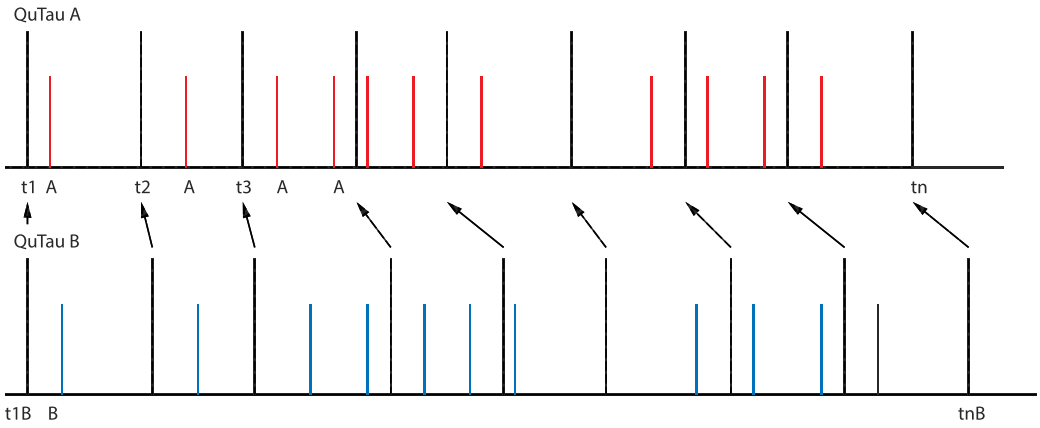

Figure 3.12: Here the example of a single slot. We can observe that quTau A and B register the same trigger signal at a different moment. The black lines are the trigger signals, while the colored ones refer to signal photons on channel A and B respectively.

in section 3.6. We this technique, even though we are working with different and indipendent

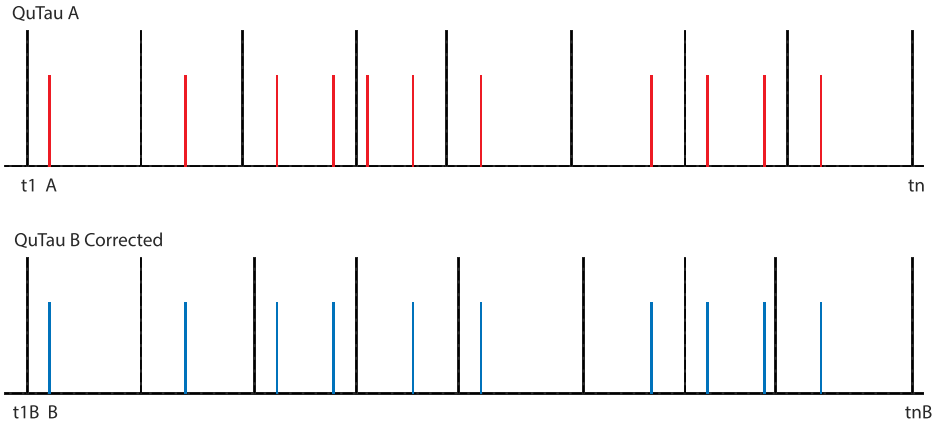

Figure 3.13: Here we corrected via software the time registred for the slot. As a consequence we observe that blue lines on channel B and red lines on channel A happen at the same time. This means that we will find them on the same coincidence window as expected before

terminals, we are able to obtain the same results that we obtained working with one TDC. This is confirmed simply by measuring the same three peaks as explained in section 3.6. Looking at figure 3.14 we observe that in both channels we have well separated peaks. In this way photons coming from long and short arms will be distinguishable, allowing us to reach a good visibility. In figure 3.15 the delay is quite long, compared with that one obtained working on a single TDC, this is due to the optical link and the electronics used for it. Finally we can assert that, thanks to the optical link, the separated and indipendent TDCs will work as a single system stable even with terminals at a great distance from each other. The optical link is a good solution to perform free-space quantum communications, when a high precision is needed.

3.3 Data Analysis

Coincidence window definition, as most data processing, are implemented with $Matlab^{®}$. In this section we will describe our the experiment results. In the first part we will introduce the methods we used, letting to the second part the data analysis.

3.3.1 Density Matrix Operator

First of all we introduce the *Density Matrix Operator*, which is a theoretical tool of great importance when talking about complex systems such as two particles hyper-entangled systems.

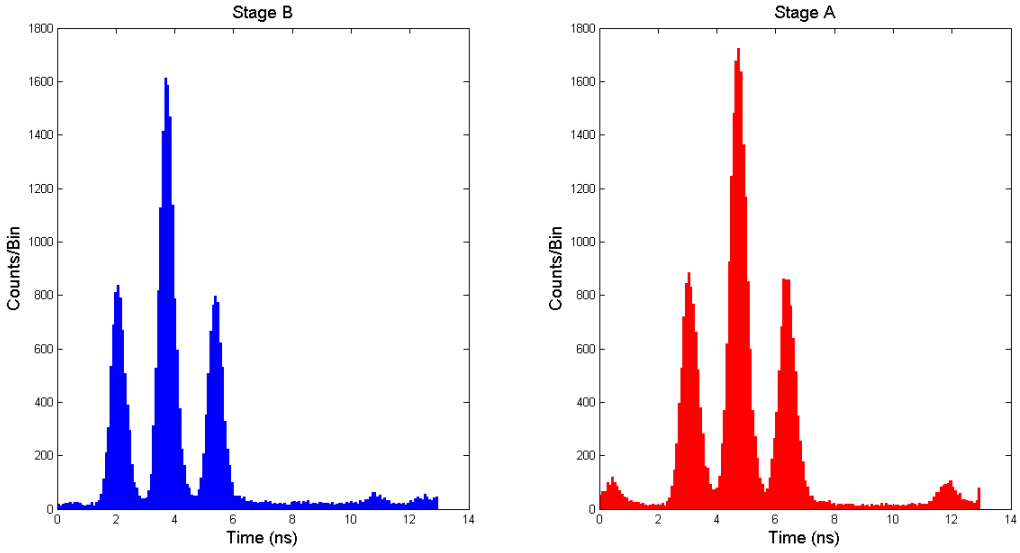

Figure 3.14: Here the histograms of time arrivals. As done in section 3.6, we obtain three peaks that are well separated. This means that we were able to synchronize well the indipendent terminals, with a high precision

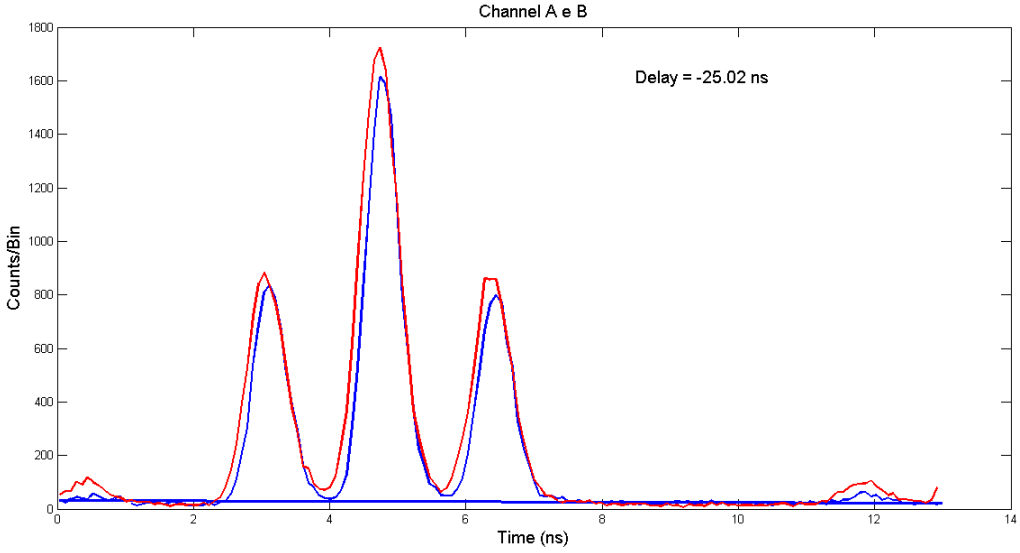

Figure 3.15: Here the histograms of time arrivals together. The difference is that now the delay is long. This is due to the optical link as well as to the electronics used to obtain the optical link.

We will see how density matrix formalism gives us a more direct interpretation of experimental results. Moreover it will give us some criteria to compare our experimental data with theoretical ones. These criteria will be also used to implement analysis methods such as *Compressive Sensing* and *Maximum Likelihood Estimates*.

Definition 3 ***(Density Matrix)*** *For a generic state $|\Psi\rangle$ written as*

$$|\Psi\rangle = \sum_{i=1}^{n} c_i |\psi_i\rangle, \tag{3.34}$$

we define ***Density Matrix*** *as an operator on the Hilbert space of the system such that*

$$\hat{\rho} = \sum_{i=1}^{n} p_i |\psi_i\rangle\langle\psi_i|, \tag{3.35}$$

where p_i are the probabilities of finding the system in the i-th state.

In general, as one can see from (3.35), $\hat{\rho}$ will be *Hermitian*. We immediately observe some conditions that probabilities satisfy:

$$\begin{aligned} &\sum_{i=1}^{n} p_i = 1; \\ &0 \leq p_i \leq 1; \\ &\sum_{i=1}^{n} {p_i}^2 \leq 1. \end{aligned} \tag{3.36}$$

From these conditions we obtain that $\hat{\rho}$ will be *Positive Semidefinite*. Moreover, related to these probabilities, we can distinguish two different situations:

- the most general one is that of *Mixed States*, for which probabilities p_i assume different values. In this case equation (3.35) holds;
- the second situation is that of states for which we have the same probability for each eigenstate $|\psi_i\rangle$. Because of this fact we can extract the p_i and obtain

  $$\hat{\rho} = |\Psi\rangle\langle\Psi|, \tag{3.37}$$

  with $|\Psi\rangle$ the total system state. These are called *Pure States*.

We now describe some properties of $\hat{\rho}$. We first demonstrate now that either for *Mixed* and *Pure* states

$$tr\hat{\rho} = 1. \tag{3.38}$$

Consider an orthogonal base $\{\phi_k\}$ and (3.35). By definition we can write

$$\begin{aligned} tr\hat{\rho} = \sum_{k=1}\langle\phi_k|\hat{\rho}|\phi_k\rangle &= \sum_{k=1}\sum_{i=1}\langle\phi_k|p_i|\psi_i\rangle\langle\psi_i|\phi_k\rangle \\ &= \sum_{i=1} p_i\langle\psi_i|\phi_k\rangle\langle\phi_k|\psi_i\rangle \\ &= \sum_{i=1} p_i = 1; \end{aligned}$$

where we have used (3.36) and the completeness relation. As we have not put any condition on p_i values, this equation holds both for mixed and pure states. Hence, it cannot help us to distiguish between them.
Now we demonstrate that the square of density operator allows us to distinguish between pure and mixed states. For pure states we have, by definition

$$\hat{\rho}^2 = (|\Psi\rangle\langle\Psi|)\,(|\Psi\rangle\langle\Psi|) = |\Psi\rangle\langle\Psi| = \hat{\rho}. \tag{3.39}$$

Furthermore we have

$$tr\hat{\rho}^2 = tr\hat{\rho} = 1. \tag{3.40}$$

Things changes when we deal with mixed states as we get

$$\hat{\rho}^2 = \sum_{i,j=1} p_i p_j |\psi_i\rangle\langle\psi_i|\psi_j\rangle\langle\psi_j|. \tag{3.41}$$

We then calculate the trace

$$\begin{aligned} tr\hat{\rho}^2 &= \sum_{k=1}\sum_{i,j=1} p_i p_j \langle\phi_k|\psi_i\rangle\langle\psi_i|\psi_j\rangle\langle\psi_j|\phi_k\rangle \\ &= \sum_{i,j=1} p_i p_j |\langle\psi_j|\psi_i\rangle|^2 \\ &\leq \left[\sum_{i=1}^{n} p_i\right]^2 = 1. \end{aligned} \tag{3.42}$$

It is worth noting that the equality holds only if $\langle\psi_j|\psi_i\rangle = 1$ for every i and j. This would happen with vectors that differ for a phase factor, but since states are defined by vector ray on an Hilbert space, in this situation we would deal again with pure states. Thus we reach the conclusion that

$$\begin{aligned} &tr\hat{\rho}^2 = 1 \quad \text{for pure states} \\ &tr\hat{\rho}^2 < 1 \quad \text{for mixed states.} \end{aligned} \tag{3.43}$$

We have demonstrated that we have a criterion to check the *purity* of our state. We are led to define

$$P = tr\hat{\rho}^2, \tag{3.44}$$

expecting to obtain an experimental P value a little lower (because of experimental errors) than 1. As we have said above, density matrix formalism allows us to compare more directly experimental results with theoretical models. This goal is achieved, in particular, with the relation

$$\langle \hat{O} \rangle = tr(\hat{\rho}\hat{O}), \tag{3.45}$$

where $\hat{O}$ is a generic operator acting on the Hilbert space of the system. The expectation value of $\hat{O}$ is defined as

$$\langle \hat{O} \rangle = \sum_k \langle \phi_k | \hat{O} | \phi_k \rangle. \tag{3.46}$$

Using completeness relation on the $\{\psi_i\}$ base and $\hat{\rho}$ definition, we can write

$$\begin{aligned}
\langle \hat{O} \rangle &= \sum_k \sum_i \langle \phi_k | \psi_i \rangle \langle \psi_i | \hat{O} | \phi_k \rangle \\
&= \sum_k \langle \phi_k | \left(\sum_i \psi_i \rangle \langle \psi_i | \hat{O} \right) | \phi_k \rangle \\
&= \sum_k \langle \phi_k | \hat{\rho}\hat{O} | \phi_k \rangle \\
&\equiv tr(\hat{\rho}\hat{O}).
\end{aligned}$$

3.3.2 Density Matrix in our experiment

In the previous subsection we have introduced density matrix operator, showing its most important properties. Now we will focus on density matrix expected for our experiment, describing the different results we could obtain. We first write density matrices for polarization and time DOFs separated and then we write the hyper-entangled state density matrix. To do so, it is useful to write our polarization and time entangled states

$$|\Psi\rangle = \frac{1}{\sqrt{2}} \left(|H\rangle_A |V\rangle_B - |V\rangle_A |H\rangle_B \right) \tag{3.47}$$

and

$$|\tau\rangle = \frac{1}{\sqrt{2}} \left(|S\rangle_A |S\rangle_B - |L\rangle_A |L\rangle_B \right). \tag{3.48}$$

We then calculate density matrix operator for $|\Psi^{\pm}\rangle$ and $|\tau\rangle$. By definition we have

$$\begin{aligned}
\hat{\rho}_P &= |\Psi^-\rangle\langle\Psi^-| \\
&= \frac{1}{2} \left(|H\rangle_A |V\rangle_B - |V\rangle_A |H\rangle_B \right) \left(\langle H|_A \langle V|_B - \langle V|_A \langle H|_B \right).
\end{aligned}$$

This relation can be expressed as a 4x4 matrix

$$\hat{\rho}_P = \frac{1}{2}\begin{pmatrix} 0 & 0 & 0 & 0 \\ 0 & 1 & -1 & 0 \\ 0 & -1 & 1 & 0 \\ 0 & 0 & 0 & 0 \end{pmatrix} \tag{3.49}$$

For time-entangled state we get

$$\hat{\rho}_T = |\tau\rangle\langle\tau| \tag{3.50}$$

that, written in matrix form, becomes

$$\hat{\rho}_T = \frac{1}{2}\begin{pmatrix} 1 & 0 & 0 & -1 \\ 0 & 0 & 0 & 0 \\ 0 & 0 & 0 & 0 \\ -1 & 0 & 0 & 1 \end{pmatrix} \tag{3.51}$$

The hyper-entangled state is given by

$$|\Xi\rangle = |\Psi^-\rangle \otimes |\tau\rangle. \tag{3.52}$$

The density matrix will be a 16x16 matrix, tensor product of the separated matrices. We observe that a 16x16 matrix implies 256 matrix elements that corresponds to 256 measures as one can check by (3.45).

3.3.3 Quantum Tomography

As presented above, one of the main goals of our experiment is to make a *Quantum State Tomography* of time-polarization hyper-entangled states. *Quantum State Tomography* is a process that aims to reproduce quantum states density matrix. Now we show how the necessary information is recovered from experimental data. We remind that in this case, experimental data correspond to coincidence counts in the measurement apparatus. We follow arguments presented in Kwiat et al. (2001) [20].
In the following we will take advantage of density matrix formalism and *Stokes parameters*, which are experimental parameters that allow a complete description of classical light beam. In 1852, George Stokes proposed a method to fully characterize light beams. It consisted of some, properly chosen, measurements. He found out that it sufficed to measure light with

- a 50:50 polarization indipendent filter;
- a horizontal polarized filter;
- a polarized filter rotated of 45° from horizontal one;

- a filter which transmitted only right-circular polarization.

In this way he would have achieved the necessary information to describe light beams. These measurements can be expressed in terms of quantum states, that we write as combination of $|L\rangle$ and $|R\rangle$ eigenstates.

$$\begin{aligned} n_0 &= \frac{\mathcal{N}}{2}\left(\langle H|\hat{\rho}|H\rangle + \langle V|\hat{\rho}|V\rangle\right) = \frac{\mathcal{N}}{2}\left(\langle R|\hat{\rho}|R\rangle + \langle L|\hat{\rho}|L\rangle\right) \\ n_1 &= \mathcal{N}\langle H|\hat{\rho}|H\rangle = \frac{\mathcal{N}}{2}\left(\langle R|\hat{\rho}|R\rangle + \langle L|\hat{\rho}|L\rangle + \langle R|\hat{\rho}|L\rangle + \langle L|\hat{\rho}|R\rangle\right) \\ n_2 &= \mathcal{N}\langle A|\hat{\rho}|A\rangle = \frac{\mathcal{N}}{2}\left(\langle R|\hat{\rho}|R\rangle + \langle L|\hat{\rho}|L\rangle + i\langle R|\hat{\rho}|L\rangle - i\langle L|\hat{\rho}|R\rangle\right) \\ n_3 &= \frac{\mathcal{N}}{2}\langle R|\hat{\rho}|R\rangle. \end{aligned} \tag{3.53}$$

Stokes parameter are then defined as

$$\begin{aligned} \mathcal{S}_0 &= 2n_0 = \mathcal{N}\left(\langle R|\hat{\rho}|R\rangle + \langle L|\hat{\rho}|L\rangle\right) \\ \mathcal{S}_1 &= 2\left(n_1 - n_0\right) = \mathcal{N}\left(\langle R|\hat{\rho}|L\rangle + \langle L|\hat{\rho}|R\rangle\right) \\ \mathcal{S}_2 &= 2\left(n_2 - n_0\right) = \mathcal{N}i\left(\langle R|\hat{\rho}|L\rangle - \langle L|\hat{\rho}|R\rangle\right) \\ \mathcal{S}_3 &= 2\left(n_3 - n_0\right) = \mathcal{N}\left(\langle R|\hat{\rho}|R\rangle - \langle L|\hat{\rho}|L\rangle\right). \end{aligned} \tag{3.54}$$

In this way we can express density matrix in terms of Stokes parameters as

$$\hat{\rho} = \frac{1}{2}\sum_{i=0}^{3}\frac{\mathcal{S}_i}{\mathcal{S}_0}\hat{\sigma}_i, \tag{3.55}$$

where Pauli operators are projectors related to linear combinations of polarization eigenstates. This is the first step that will allow us to obtain multi-qubit tomography. In fact it can be shown that for a multi-qubit system we can write density matrix as

$$\hat{\rho} = \frac{1}{2^n}\sum_{i_1,..,i_n=0}^{3}\frac{\mathcal{S}_{i_1,..,i_n}}{\mathcal{S}_{0,..,0}}\hat{\sigma}_{i_1}\otimes ... \otimes \hat{\sigma}_{i_n}. \tag{3.56}$$

This represents a good result that will always work correctly for a complete set of measurements. However it could happen that we want to modify the choice of our measurements. Sometimes, in fact, we would prefer to measure different states, maybe because of experimental pratical reasons. This situation need another approach that will give us a method to characterize complete set of measurements. The complete method can be find in [Kwiat2001]. We just say that in this case the completeness of measurements set can be checked by verifying that a given matrix is not singular. For a two qubit systems that matrix is a 16x16 matrix.

This fact suggests that for polarization-time hyper-entangled states we would need a 256x256 matrix. However with this method we get, for our hyper-entangled state,

$$\hat{\rho} = \frac{1}{\mathcal{N}} \sum_{\nu=1}^{256} M_\nu n_\nu, \tag{3.57}$$

with $\mathcal{N}$ given by

$$\mathcal{N} = \sum_{\nu=1}^{16} n_\nu. \tag{3.58}$$

In this case M_ν are related to measurements operators in a given base and are 16x16 matrices, while n_ν are the measurements results, that from a theoretical point of view are described by (3.45). Hence we have proposed a first method to exploit tomography method recover density matrix.
It is important to point out that (3.57) is just the starting point of density matrix recovering. In fact it could happen that it does not satisfy some *physical conditions*, needed for density matrices. As done talking about density matrix operator we can sum up these properties as

- normalization: $tr\hat{\rho} = 1$;
- semipositive definiteness;
- hermiticy.

These condition are necessary to evaluate experimental results. First condition help us to check that probabilities sum is one and thus let us check that measurements are correct, while second and third conditions imply that $tr\hat{\rho}^2 \leq 1$, and consequentely give us a method to check the purity of our state. Unfortunately these condition are not always verified when using the method proposed above. In this particular case *Maximum Likelihood Method* can help us.

3.3.4 Maximum Likelihood

Our Maximum likelihood method has the following basic idea: starting from a set of experimental data, one wants to find out the associated density matrix that get more close to that data, while preserving some physical condition. In doing so we define a density matrix $\hat{\rho}_{ph}(t_1, .., t_{256})$, ("ph" stands for physical) that preserves *Normalization*, *Semipositive Definiteness* and *Hermiticy* properties, and will depend on a set of 256 parameters $\{t_\nu\}$. A method to get a 256 parameters complex matrix that preserves these properties is to define a proper $\hat{T}$ triangular matrix and calculate

$$\hat{\rho}_{ph} = \frac{\hat{T}^\dagger(t)\hat{T}(t)}{tr\left[\hat{T}^\dagger(t)\hat{T}(t)\right]}. \tag{3.59}$$

One then calculates the probability density that an experimental measurement is close to any matrix element $\langle\psi_\nu|\hat{\rho}_{ph}|\psi_\nu\rangle$, where in this case $|\psi_\nu\rangle$ are 256 measurement states. If one suppose that no systematic errors occur, experimental data will have a gaussian distribution around the corresponding matrix element. What we want to maximize is the product of all gaussian density distributions, one for each experimental measurement.

$$\mathcal{P}(t_1,..,t_{256}) = \frac{1}{N_{norm}} \prod_{\nu=1}^{256} exp\left[-\left(\frac{\mathcal{N}\langle\psi_\nu|\hat{\rho}_{ph}|\psi_\nu\rangle - n_\nu}{2\mathcal{N}\langle\psi_\nu|\hat{\rho}_{ph}|\psi_\nu\rangle} \right)^2 \right]. \tag{3.60}$$

A simpler calculation is obtained by maximizing its logarithm with sign changed, which gives

$$\mathcal{L}(t_1,..,t_{256}) = \sum_{\nu=1}^{256} \left(\frac{\mathcal{N}\langle\psi_\nu|\hat{\rho}_{ph}|\psi_\nu\rangle - n_\nu}{2\mathcal{N}\langle\psi_\nu|\hat{\rho}_{ph}|\psi_\nu\rangle} \right)^2. \tag{3.61}$$

Thus, our goal is to find the set $\{t_\nu\}$ which minimize $\mathcal{L}(t_1,..,t_{256})$. As proposed by Kwiat, we use *Mathematica*® routine *"FindMinimum"* to achieve this goal.

3.3.5 Compressive Sensing

In Quantum Physics size of systems grows exponentially with the total number of DOFs considered. This implies that even the number of matrix elements of density matrices will grow exponentally. Consider, for example a couple of particles entangled in polarization. We have $d = 2^{2n}$, where n is the total number of DOFs, and "2" is the base's dimension for polarization states. In this case our density matrix will have 16 entries. If we add time-entangled part, we get $n = 4$ and consequentely $d = 256$. If, for example, we would add a new two levels' degree of freedom to our time-polarization hyper-entangled state, we would need $d = 2^{12} = 4096$ measurements to represent our density matrix. It is easy to understand that making 4096 measurements could be very difficult and obviusly time expensive. Moreover if we want to exploit quantum technology we have to be able to characterize quantum systems with more than 3 or 4 qubits.
We are thus interested in finding methods that, without loosing too much information on the system, allow us to recover the density matrix. Compressive sensing is what we are looking for to solve such a problem.

Compressive sensing method comes from signal processing. It was originally employed to recover vectors that were **sparse** in some bases. The basic idea was that if a vector has a great part of zero entries, then it will suffices to do few measures to get most information contained in such vector. This method has then been brought, with some differences, to matrix reconstructing methods and applied to Quantum State Tomography.
Here the idea remains almost the same: if a matrix is low-rank, then about $O(rd)$ measurements will allow to reconstruct it, where r is rank and d the matrix dimension. A rigorous

result has been demonstrated in 2010 [21]. It describes the above idea in a formal way. Given the convex optimization problem

$$\begin{cases} \textit{minimize} \ \ ||\hat{\rho}||_{tr} \\ \text{s.t.} \ \ tr(\hat{\rho}\hat{M}_i) = tr(\hat{\rho}_{exp}\hat{M}_i), \quad i = 1, .., m \\ \hat{\rho} \succeq 0 \end{cases} \tag{3.62}$$

with $\hat{\rho}$ hermitian matrix and $\hat{M}_i$ a random sampled measure from the complete set, the following theorem has been demonstrated

Theorem 1 *Consider a low-rank matrix $\hat{\rho}$, with rank r and dimension d. Then, with a failure probabability exponentially small in c, $m = crd(log^2 d)$ measurements will suffice to recover the density matrix $\hat{\rho}$.*

However, because this result cannot be used with noisy data, the method is not useful in real experiments. Moreover, we will never deal with low-rank matrices, but always with approximately low-rank matrices. In the same article Gross proposes a method that is robust against noise and allows to work with experimental real data. This method, valid for almost pure states, is written as

$$\begin{cases} \textit{minimize} \ \ ||\hat{\rho}||_{tr} \\ \text{s.t.} \ ||tr(\hat{\rho}\hat{M}_i) - b_i||_2 < \varepsilon, \quad i = 1, .., m \\ \hat{\rho} \succeq 0 \end{cases} \tag{3.63}$$

where b_i are the noisy experimental data and ε is related to the experimental error. In this case the number of necessary measures is a little greater than that proposed in theorem (1).
This technique is based on Semidefinite Programming (SDP) methods, implemented with Yalmip® tools, that interface with $Matlab$®.

Chapter 4

Experimental Results

In this section we report results obtained in our experiment. In this case we show that we can obtain a Bell inequality violation using polarization and time separated. Then we show two quantum state tomographies for both time and polarization. For polarization we connect the fiber optic, exiting the polarization stage directly to the SPAD avoiding the interferometers. In this way we can obtain greater counts that allow us to have a lower error. When measuring time states we project the polarization entangled state on the eigenstate $|H\rangle|V\rangle$. We let to the second part the results about hyper-entangled quantum state tomography.

4.1 Bell Measurements

In the following discussion we take advantage of arguments developed in section 1.2.1. We have to measure

$$S_{exp}(\alpha, \beta, \alpha', \beta') = E_{exp}(\alpha, \beta) - E_{exp}(\alpha', \beta) + E_{exp}(\alpha, \beta') + E_{exp}(\alpha', \beta'), \tag{4.1}$$

where

$$E_{exp}(\alpha, \beta) = \frac{C_{exp}(\alpha, \beta) - C_{exp}(\alpha_\perp, \beta) - C_{exp}(\alpha, \beta_\perp) + C_{exp}(\alpha_\perp, \beta_\perp)}{C_{exp}(\alpha, \beta) + C_{exp}(\alpha_\perp, \beta) + C_{exp}(\alpha, \beta_\perp) + C_{exp}(\alpha_\perp, \beta_\perp)} \tag{4.2}$$

and C_{exp} indicates the experimental counts for a given choice of angles, which are reported in Tab. (4.1).

Bell's Inequality for polarization state

In Tab. (4.3) we write counts for each combination of angles in A and B channel. The order is chosen to allow us to make a minor number of wave plates rotations. In this way we have a lower experimental error when changing position.

α	$\frac{\pi}{2}$	$\alpha_\perp$	0
α'	$-\frac{\pi}{4}$	$\alpha'_\perp$	$\frac{\pi}{4}$
β	$\frac{3\pi}{8}$	$\beta_\perp$	$\frac{7\pi}{8}$
β'	$-\frac{3\pi}{8}$	$\beta'_\perp$	$\frac{\pi}{8}$

Table 4.1: Angles for Bell inequality experimental test

	α	$\alpha_\perp$	α'	$\alpha'_\perp$
β	16246 ± 127	2914 ± 54	16566 ± 129	2879 ± 54
$\beta_\perp$	2844 ± 53	14900 ± 122	2623 ± 51	16229 ± 127
β'	16225 ± 127	2450 ± 50	3025 ± 55	15794 ± 126
$\beta'_\perp$	2761 ± 53	16303 ± 128	15968 ± 126	2867 ± 54

Table 4.2: Counts obtained to test Bell inequality. Here we consider only polarization observable.

For this choice of angles a classical LHV theory, as that reported in section (1.2.1), reaches its maximum value $S_{th} = 2$. Using relations (4.1) and (4.2) we obtain

$$S_{exp} = 2,8115 \pm 0,0075. \tag{4.3}$$

The E_i values were in that case

$$\begin{aligned} E1 &= 0.6869 \pm 0.0038 \\ E2 &= 0.7238 \pm 0.0036 \\ E3 &= 0.7127 \pm 0.0037 \\ E4 &= -0.6870 \pm 0.0038 \end{aligned} \tag{4.4}$$

where we have poissonian errors. We obtain a strong violation of classical limits.

Bell's Inequality for time state

As done for polarization, we write counts for each combination of angles in A and B channel. The order now is chosen to allows us to make a minor slides' movements. In this way we have a lower experimental error when changing position. Using relations (4.1) and (4.2) we obtain

	α	$\alpha_\perp$	α'	$\alpha'_\perp$
β	532 ± 23	73 ± 9	498 ± 22	86 ± 9
$\beta_\perp$	90 ± 9	513 ± 23	104 ± 10	510 ± 23
β'	509 ± 23	108 ± 10	86 ± 9	514 ± 23
$\beta'_\perp$	92 ± 10	498 ± 23	537 ± 24	98 ± 10

Table 4.3: Counts obtained to test Bell inequality. Here we consider time-bin observable.

$$S_{exp} = 2,7836 \pm 0,0414. \tag{4.5}$$

The E_i values were in that case

$$\begin{aligned} E1 &= 0.7301 \pm 0.0197 \\ E2 &= 0.6686 \pm 0.0214 \\ E3 &= 0.6828 \pm 0.0209 \\ E4 &= -0.7020 \pm 0.0207 \end{aligned} \tag{4.6}$$

where we have poissonian errors. We obtain a strong violation of classical limits. Here we can observe a greater error. This is due to the lower counts, which entail a greater relative poissonian error.

4.2 Experimental Quantum State Tomography

In this section we report results about quantum state tomographies. At first we consider polarization and time separated, obtaining two different 4x4 density matrices. Then we pass to the 16x16 density matrix for the hyper-entangled state.

Quantum State Tomography: Polarization

In tab. (4.4) we report experimental counts with the corrensponding measure. Performing a Quantum State Tomography we obtain, with Maximum Likelihood Estimates, the density matrix (4.7).

$$\hat{\rho}_{pol} = \begin{pmatrix} 0.0051 & -0.031 - 0.003i & 0.032 + 0.001i & 0.006 - 0.003i \\ -0.032 + 0.003i & 0.497 & -0.492 + 0.023i & -0.040 + 0.004i \\ 0.032 - 0.001i & -0.492 - 0.024i & 0.488 & 0.040 - 0.002i \\ 0.006 + 0.002i & -0.039 - 0.004i & 0.040 + 0.002i & 0.009 \end{pmatrix} \tag{4.7}$$

Here we list some important parameters, that characterized the recoverd matrix. The Fidelity, for pure states is defined as

$$\mathcal{F} = Re\{Tr(\hat{\rho} \cdot \hat{\rho}_{ideal})\} \tag{4.8}$$

Another important parameter is the Purity that expresses how the recovered state is close to the ideal pure state, and it is defined as

$$\mathcal{P} = Re\{Tr(\hat{\rho} \cdot \hat{\rho})\} \tag{4.9}$$

In the case of polarization the ideal matrix has the form in eq. (4.12)

$$\hat{\rho}_{ideal} = \frac{1}{2} \begin{pmatrix} 0 & 0 & 0 & 0 \\ 0 & +1 & -1 & 0 \\ 0 & -1 & +1 & 0 \\ 0 & 0 & 0 & 0 \end{pmatrix} \tag{4.10}$$

Then, calculating fidelity and purity, we obtain for polarization states

$$\begin{cases} \mathcal{F}_{pol} & = 98.52 \pm 0.02\% \\ \mathcal{P}_{pol} & = 98.23 \pm 0.03\%. \end{cases} \tag{4.11}$$

Density matrices for all physical states must have the property of positive semidefiniteness which, in conjunction with the normalization and hermiticity properties, implies that all of

the eigenvalues must lie in the interval [0,1] their sum being 1. This in turn implies that $0 \leq Tr\hat{\rho}^2 \leq 1$. Thus the purity makes us sure that we have recovered a density matrix with the correct physical properties. Simple calculations show that the recovered matrix is normalized and it has also positive eigenvalues.

State	Counts
$\|H\rangle\|H\rangle$	0
$\|H\rangle\|V\rangle$	451±21
$\|V\rangle\|V\rangle$	5±2
$\|V\rangle\|H\rangle$	443±21
$\|R\rangle\|H\rangle$	208 ±14
$\|R\rangle\|V\rangle$	213±14
$\|D\rangle\|V\rangle$	191±13
$\|D\rangle\|H\rangle$	250±15
$\|D\rangle\|R\rangle$	246±15
$\|D\rangle\|D\rangle$	10±3
$\|R\rangle\|D\rangle$	226±15
$\|V\rangle\|D\rangle$	196±14
$\|H\rangle\|D\rangle$	260±15
$\|V\rangle\|L\rangle$	225±15
$\|H\rangle\|L\rangle$	228±15
$\|R\rangle\|L\rangle$	459±21

Table 4.4: Counts obtained to perform a quantum state tomography. Here we consider only polarization observable.

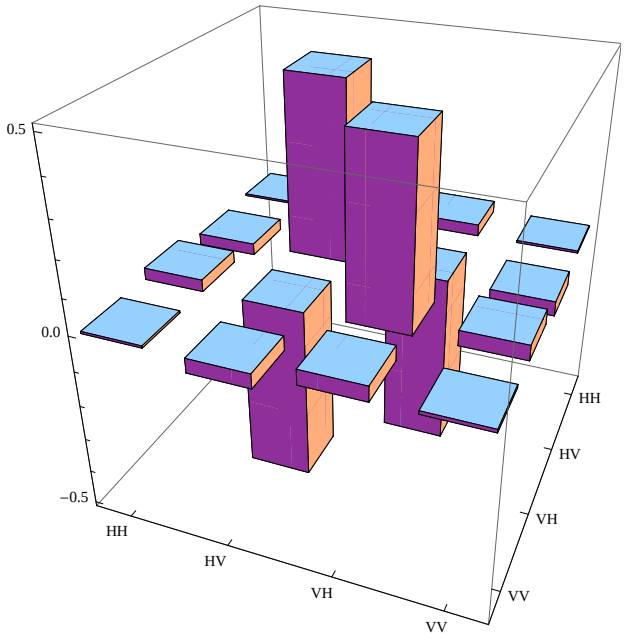

Figure 4.1: Here the real part of the recovered density matrix. We observe e strong similarity to the ideal matrix.

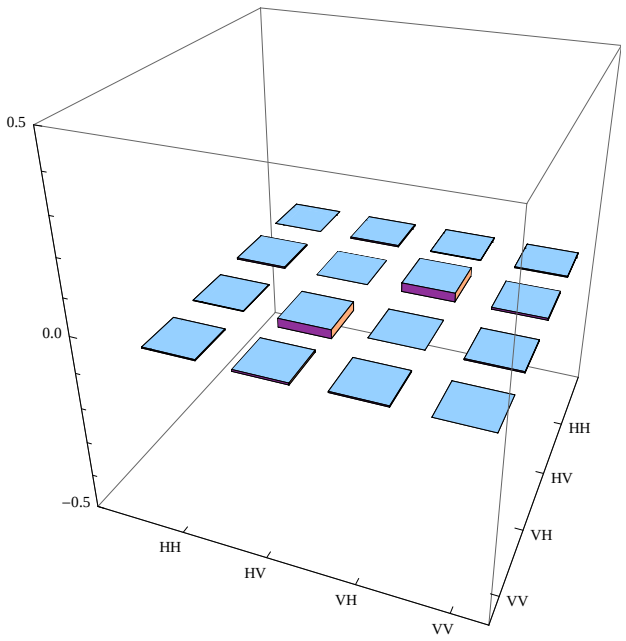

Figure 4.2: Here the imaginary part. Low values imply that our state is closed to a pure state.

Quantum State Tomography: Time

In that case we perform the same analysis that we did for polarization states. However we have a different state and the ideal density matrix in this case is given by

$$\hat{\rho}_{ideal} = \frac{1}{2}\begin{pmatrix} +1 & 0 & 0 & -1 \\ 0 & 0 & 0 & 0 \\ 0 & 0 & 0 & 0 \\ -1 & 0 & 0 & +1 \end{pmatrix} \tag{4.12}$$

The measured counts, with the corrensponding states are reported in tab. (4.5), as done for polarization. In tab. (4.14) we report the recovered density matrix for time states. In that case

State	Counts
$\|L\rangle\|L\rangle$	471± 22
$\|L\rangle\|S\rangle$	5±2
$\|S\rangle\|S\rangle$	534±23
$\|S\rangle\|L\rangle$	0
$\|R\rangle\|L\rangle$	254 ±15
$\|R\rangle\|S\rangle$	256±15
$\|D\rangle\|S\rangle$	278±16
$\|D\rangle\|R\rangle$	239±15
$\|D\rangle\|R\rangle$	228±15
$\|D\rangle\|D\rangle$	14±3
$\|R\rangle\|D\rangle$	256±16
$\|S\rangle\|D\rangle$	231±15
$\|L\rangle\|D\rangle$	250±15
$\|V\rangle\|Left\rangle$	259±16
$\|H\rangle\|Left\rangle$	238±15
$\|R\rangle\|Left\rangle$	15±4

Table 4.5: Counts obtained to perform Quantum State Tomography. Here we consider only time-bin observable.

we obtained for the fidelity and the purity

$$\begin{cases} \mathcal{F}_{time} &= 97.12 \pm 0.02\% \\ \mathcal{P}_{time} &= 94.85 \pm 0.04\%. \end{cases} \tag{4.13}$$

$$\hat{\rho}_{time} = \begin{pmatrix} 0.461 & 0.004 + 0.005i & 0.001 - 0.019i & -0.487 + 0.027i \\ 0.004 - 0.005i & 0.003 & -0.001 - 0.004i & 0.007 + 0.007i \\ 0.001 + 0.019i & -0.001 + 0.004i & 0.005 & -0.008 - 0.007i \\ -0.48 - 0.027i & 0.007 - 0.007i & -0.007 + 0.007i & 0.526 \end{pmatrix} \tag{4.14}$$

Again the purity makes us sure that we have recovered a density matrix with the correct physical properties. As for polarization states we have recovered a normalized density matrix with positive eigenvalues.

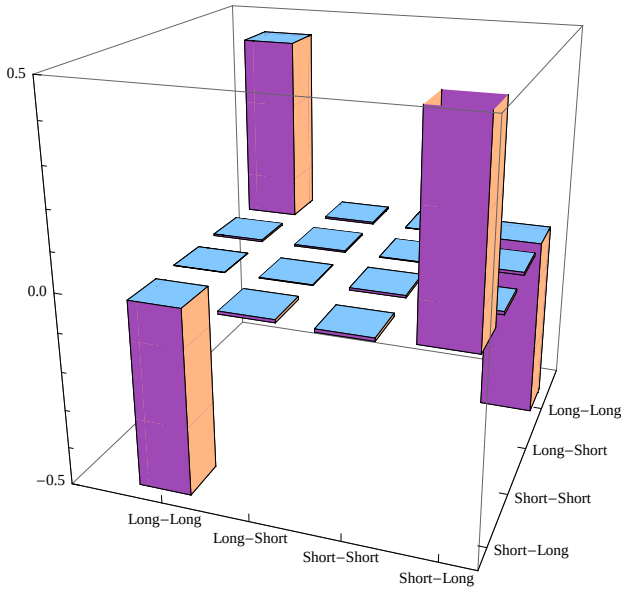

Figure 4.3: Here the real part. The different matrix is due to a different state, which expression has been defined in the previous chapters.

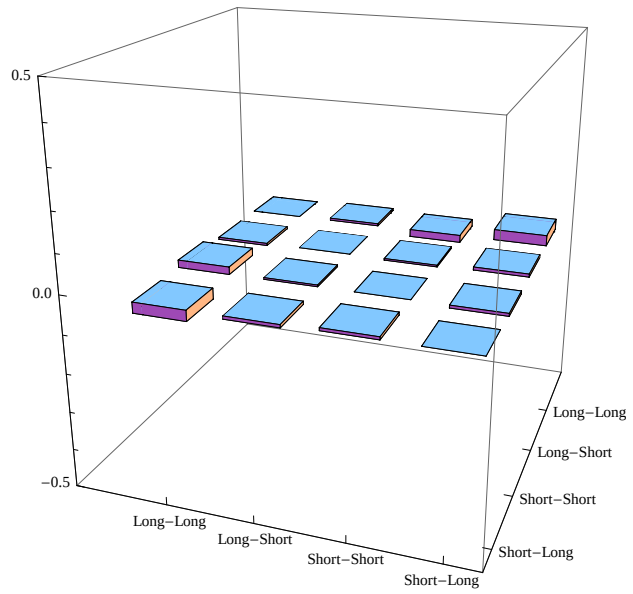

Figure 4.4: Here the imaginary part. Again we observe low values that indicate that our state is close to a pure one

Quantum State Tomography: Hyper-entanglement

The previous sections were necessary to be sure that we were dealing with photons entangled both in polarization and time. Once we have checked this, we are ready to perform a complete quantum state tomography. In this case, as said before we exploit the Compressive Sensing Method. In that case we limited to 145 measurements, chosen randomly from the over-complete set of possible measurements defined by the combination of the eigenstates $|S\rangle, |L\rangle, |D\rangle, |A\rangle, |Right\rangle, |Left\rangle$. With this number of measurementes we were able to obtain

$$\begin{cases} \mathcal{F} &= 91.13 \pm 0.05\% \\ \mathcal{P} &= 85.98 \pm 0.04\%. \end{cases} \tag{4.15}$$

At first we report the histogram for the ideal density matrix, in order to compare our results with the ideal ones. Discussing about compressive sensing it is interesting to look for the number of measures needed to obtain such values of fidelity and purity. To do so, we plot the fidelity as a function of the number of measurements used. The plotted purity would be similar to the fidelity

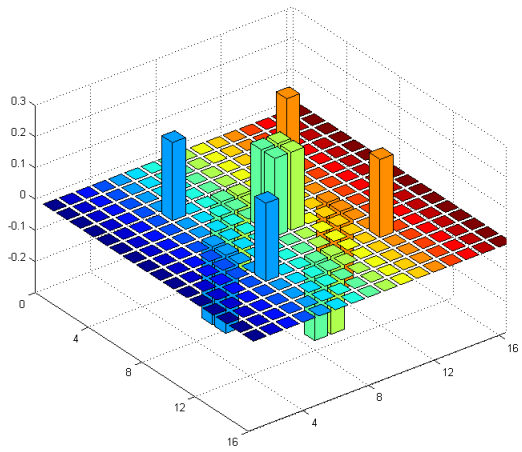

Figure 4.5: Here the ideal density matrix for the Hyper-entangled state. Each density matrix corrensponds to the hyper-entangled projected on a particular eigenstate. The order along each axis for the eigenstates is the same used for single DOF tomographies.

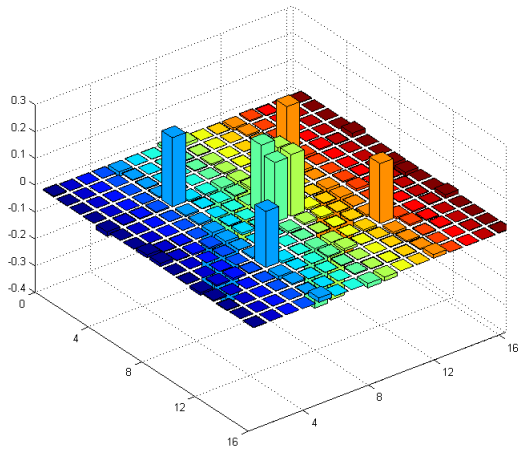

Figure 4.6: Here the recovered real part for the density matrix. A strong similarity on the matrix elements guarantees us that we measured an hyper-entangled state

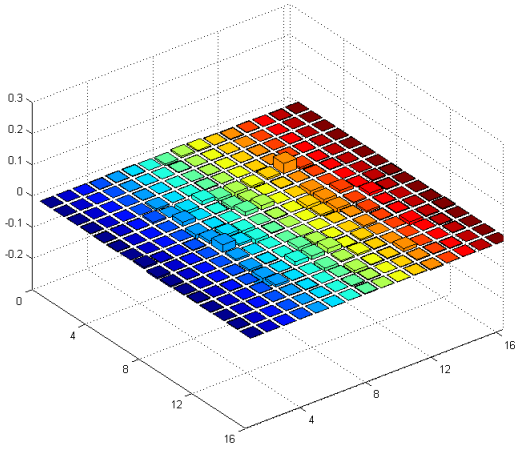

Figure 4.7: Here the recovered imaginary part for the density matrix. Low non-zero matrix elements for the imaginary part. This fact indicates that we produced a state close to a pure one.

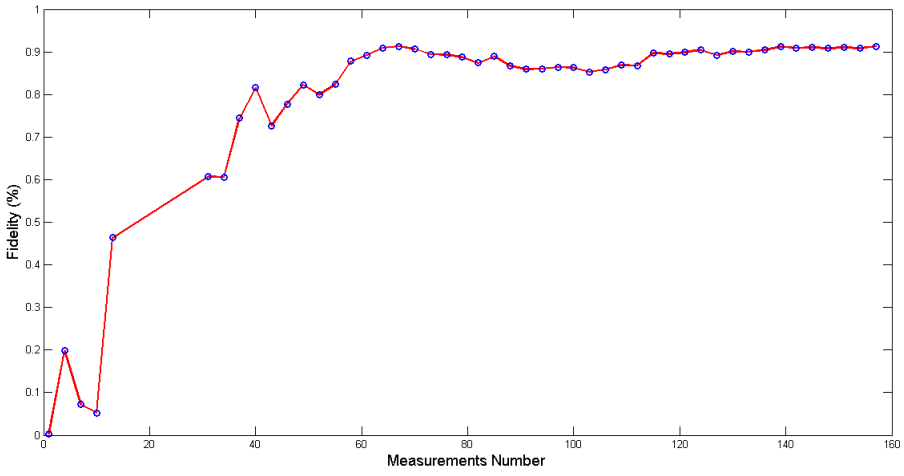

Figure 4.8: Here the fidelity as a function of the number of measurements. It is interesting to observe that about 60 measurements would suffice to achieve a 91% fidelity value.

Conclusion

With this project I demonstrated that quantum communications with polarization and time-bin hyper-entangled states between indipendent terminals are possible. The main steps toward my goal have been the following ones.

- As a first step I developed an optical system that, exploiting in input a pulsed laser source, created photons' pairs that were entangled both in polarization and time-bin. Moreover I built up two identical measurement terminals.
- Then I developed a method to synchronize separated and indipendent measurement terminals. This method was based on an optical link which acted as a reference frame for the entire system and that made me able to compare data from two separated terminals with a great precision on time registration.
- After this I performed different protocols useful to characterized quantum states. At first, working on time-bin and polarization at a different time, I was able to violate the Bell's Inequality, obtaining a result close to the quantum mechanical expected value.
- Then I performed different Quantum State Tomographies that are techniques that allow to recover quantum states' density matrices. At the beginning, as done for Bell's measurements, I worked with polarization and time-bin separately, obtaining two matrices close to the ideal ones. In that case I used Maximum Likelihood Method, that guarantees the necessary physical properties such as normalization, hermiticy and semipositive definiteness.
- In the latest part of my work I considered, at the same time, polarization and time-bin degrees of freedom. In this way, exploiting Compressive Sensing Methods, I was able to recover the density matrix for the hyper-entangled state.

These different results show that I was able to send the hyper-entangled quantum state from the source to the indipendent terminals, preserving the hyper-entanglement between the generated photons. It is important to underline the good results related with the synchronization method and time-bin entanglement. In fact the synchronization technique allow to reach the precision of hundreds picoseconds with a simple set up, while time-bin states are a good way to perform efficient quantum communications in free space. Finally my project is to be considered the

first step to achieve free-space quantum protocols such as Quantum Key Distribution or Dense Coding. In this project I worked on an optical table in which the measurement parties were indipendent but close to each other. A possible step is to perform this experiment in which one of the terminals is far away from the source. The apparatus is robust and I expect that this further step is possible in the next future.

Bibliography

[1] A. Einstein, B. Podolsky, N. Rosen, Can quantum mechanics description of physical reality be considered complete?, Physical Review, vol. 47, 1935

[2] J.S Bell, On the Einstein Podolsky Rosen Paradox, Physical Publishing Co., Vol.1, pages 195-200, 1964.

[3] Clauser et al., Proposed Experiment to Test Local Hidden-Variable Theories, Phys. Rev. Lett., vol. "23", pages 880-884, American Physical Society", 1969.

[4] Aspect et al., Experimental Test of Bell's Inequalities Using Time- Varying Analyzers, Phys. Rev. Lett., vol. 49, pages 1804-1807, 1982

[5] Franson, J. D., Bell inequality for position and time ,Phys. Rev. Lett." vol. 62, American Physical Society", 1989.

[6] Mattle K. Weinfurter H. and Kwiat P. G. Zeilinger, A., Dense Coding in Experimental Quantum Communication, Phys. Rev. Lett., vol. 76, pages 4656-4659, 1996.

[7] Bennett Brassard, G. and Crepeau, C. and Jozs, R. and Peres A., Teleporting an unknown quantum state via dual classical and Einstein-Podolsky-Rosen channels, Phys. Rev. Lett., vol. 70, pages 1895-1899, 1993.

[8] Experimental quantum teleportation, Bouwmeester et al., Nature, pages 575-579, 1997.

[9] Pan et al., Experimental Entanglement Swapping: Entangling Photons That Never Interacted, Phys. Rev. Lett., vol.80, pages 3891-3894, 1998.

[10] Bennett and Brassard, Quantum Cryptography: Quantum Key Distribution and Coin Tossing, Proc. of IEEE Conference on Computers, Systems and Signal Processing, New York: IEEE Press, 1984.

[11] C. H. Bennett, Quantum Cryptography Without Bell's Theorem, Physical Review Letter, 1992, American Physical Society

[12] Ursin R. et al., Entanglement-based quantum communication over 144 km, Nature Physics, 2007, pages 481-486

[13] Capraro Ivan et al., Turbulent single-photon propagation in the Canary optical link, QCMC 2012 conference proceedings, 2013.

[14] Adan Cabello, Bipartite Bell Inequalities for Hyperentangled States, Phys. Rev. Lett., vol. 97, 2006.

[15] Barbieri M. et al., Enhancing the Violation of the Einstein-Podolsky-Rosen Local Realism by Quantum Hyperentanglement, Phys. Rev. Lett., vol.97, 2006,

[16] Julio T. Barreiro, T.C. Wei, P.G. Kwiat, Beating the channel capacity limit for linear photonic superdense coding, Nature Physics, 2008

[17] Going beyond Bell's Theorem, D. M. Greenberger,M. A. Horne, A. Zeilinger, arXiv:0712.0921v1,2007

[18] N. David Mermin, Extreme quantum entanglement in a superposition of macroscopically distinct states Phys. Rev. Lett.,1990.

[19] Morton H. Rubin, Transverse correlation in optical spontaneous parametric down-conversion, Phys. Rev. A, 5349-5360, 1996,

[20] James Daniel F. V., Kwiat Paul G., Munro William J., White Andrew G., Measurement of qubits, Phys. Rev. A, 2001.

[21] Gross David et al., Quantum State Tomography via Compressed Sensing, Phys. Rev. Lett., 2010.

[22] Artur K. Ekert, Quantum cryptography based on Bell's theorem, Phys. Rev. Lett., 1991.